Proceedings of the AMS Centennial Symposium
August 8–12, 1988

Mathematical Fluid Dynamics: the Interaction of Nonlinear Analysis and Modern Applied Mathematics

ANDREW J. MAJDA

CONTENTS

1980 *Mathematics Subject Classification* (1985 *Revision*). Primary 76L05, 35L65.
Research partially supported by N.S.F. DMS 8702864, A.R.O. DAAL03-89-K-0013, O.N.R. N00014-89-J-1044, D.A.R.P.A. N00014-86-K-0759.

0-8218-0167-8 $1.00 + $.25 per page

Introduction. It is not difficult to understand the importance of research in fluid mechanics. The world that surrounds us involves both air and water, two primary examples of fluids. Problems of understanding fluid flow continue to have a fundamental role in both technological and basic scientific research. Such problems include the accurate tracking of hurricane paths, the nature of blood flow through the heart, the efficient mixing of fuel in internal combustion engines, and the flight of aircraft through the atmosphere at a wide variety of speeds. For example, these speeds range from the very high re-entry velocities of the space shuttle to the flight conditions near the speed of sound for typical commercial jumbo jets to the hazardous swirling flows generated by slow-moving airplanes landing at airports.

Applied mathematicians have been primary contributors to the theoretical understanding and explanation of phenomena in fluid flows through their research in mathematical fluid dynamics. It might surprise some readers that over the last two centuries, many luminaries in pure mathematics have made decisive contributions to mathematical fluid mechanics including Euler, Riemann, Weyl, Friedrichs, Courant, von Neumann, Kolmogorov, Hopf, and Leray among others. For example, a rather large portion of von Neumann's collected works involves his research in fluid mechanics. As an area of mathematical research, fluid mechanics provides rich examples of nonlinear partial differential equations with features of hyperbolic, elliptic, and mixed type depending on the various regimes of fluid motion being investigated. Such examples will be pointed out throughout this paper. The wonderful collection of experimental photographs in the book of Van Dyke [1] provides dramatic experimental confirmation for the diversity of nonlinear phenomena which occur in fluid flow in various regimes; we often refer to specific photographs from this book throughout the various sections of this paper when we discuss the mathematical structure.

The rapid development of high speed computers over the last forty years has irreversibly altered the way in which applied mathematicians do research in fluid mechanics. In fact, one common contemporary point of view states that detailed mathematical analysis in applied mathematics will rapidly become obsolete since soon there will be a "Cray supercomputer in every kitchen." In this paper, I will strongly advocate just the opposite viewpoint. The rapid evolution of applied mathematics through large scale computation reveals new phenomena in fluid flow, in some instances beyond the capability of experimental measurements. Explaining and controlling these complex phenomena requires new mathematical ideas from nonlinear analysis, differential equations, probability theory, and geometry which simultaneously interact in a highly interdisciplinary fashion with both methods for computation and more traditional tools of applied mathematics such as asymptotic methods. Thus, this increasingly broad interactive mode of research blends results from

(0.1)
(1) Large Scale Numerical Computation
(2) Asymptotic Modelling
(3) Qualitative Modelling
(4) Rigorous Mathematical Analysis for Prototype Problems

in explaining phenomena in fluid flow. Such a new mode of modern applied mathematics in close alliance with developments in theoretical mathematics is likely to reach a mature state by the beginning of the twenty-first century in other disciplines as well as mathematical fluid dynamics.

In the remainder of this paper, I will give several specific examples of this interdisciplinary interaction. The first section is an introduction to the elementary structure of fluid flow. I discuss the physical phenomena and mathematical theory for nonlinear sound waves and vorticity/turbulence respectively in §§2 and 3. A discussion of several interesting directions for contemporary and future research is included in both sections. Finally in §4, I discuss two specific and current examples of the interaction of large scale computing and modern mathematical theory in describing strikingly new phenomena in fluid flows.

1. The elementary mathematical structure of fluid flows.

(A) *The equations for compressible flow.* The equations of compressible fluid flow in N space dimensions are a system of $N+1$ equations for $N+1$ unknowns given by

$$\begin{aligned} &\frac{\partial \rho}{\partial t} + \operatorname{div}(\vec{m}) = 0, \\ &\frac{\partial \vec{m}}{\partial t} + \operatorname{div}\left(\frac{\vec{m} \otimes \vec{m}}{\rho}\right) + M^{-2}\nabla p(\rho) \\ &\qquad = \nu \operatorname{div}\left(\nabla\left(\frac{\vec{m}}{\rho}\right) + {}^{t}\nabla\left(\frac{\vec{m}}{\rho}\right) - \frac{2}{3} I \operatorname{div}\left(\frac{\vec{m}}{\rho}\right)\right). \end{aligned} \tag{1.1}$$

In (1.1), ρ is the fluid density while $\vec{m} = \rho\vec{v}$ is the momentum with $\vec{v} = {}^{t}(v_1, \ldots, v_N)$ the fluid velocity. The first equation in (1.1) expresses conservation of mass while the remaining N equations express conservation of momentum, i.e., a continuous analogue of Newton's law, $\vec{F} = m\vec{a}$. There are two forces exerted by a fluid on itself. The first is given by the pressure gradient, the term $\nabla p(\rho)$ on the left-hand side of (1.1) with $p(\rho)$, the pressure, a given nonlinear function of density determined from thermodynamics. For ideal fluids such as air or water, $p = A\rho^{\gamma}$ with constants A, γ satisfying $A > 0$ and $\gamma > 1$. The second force exerted by the fluid is the frictional force of relative motion of fluid molecules represented by the term on the right-hand side of (1.1)—ν is the coefficient of viscosity. The nondimensional number M is the Mach number and is a constant which we explain below. The size of M has enormous significance for the phenomena

observed in various regimes of fluid motion; however, we postpone a detailed discussion until §§3 and 4 of this paper which illustrate this point in detail. The $N \times N$ matrix $\vec{w} \otimes \vec{w}$ is the tensor product, $\vec{w} \otimes \vec{w})_{ij} = w_i w_j$, while $\nabla \vec{w}$ is the $N \times N$ matrix with rows given by ∇w_i and the divergence operator applied to a matrix acts on each row. This completes the definition of the equations for fluid flow. I have intentionally begun this section with this complex set of nonlinear equations. In fact, the reader with a more sophisticated knowledge of fluid dynamics recognizes that despite the complexity of these equations, I have ignored energy effects and entropy changes so that the equations in (1.1) are the system describing isentropic compressible flows [2, 3]. In the remainder of this section, I will use elementary mathematical ideas to display the structure of solutions of these equations which confirms some of our physical intuition. This provides a first illustration of the fashion in which mathematical ideas contribute to understanding fluid flow and also provides some necessary background for the remainder of this paper.

Our intuition suggests that the frictional effect measured by the coefficient of viscosity is extremely small in air or rapidly moving water. Experiments confirm that the coefficient of viscosity in nondimensional terms often has the size $\nu = O(10^{-4})$ to $\nu = O(10^{-8})$. These are the regimes of fluid flow we discuss in this paper. Since the terms on the right-hand side of (1.1) are complicated but multiplied by a small factor ν, formally we make the *zero-viscosity approximation* and set $\nu = 0$ to arrive at the *Compressible Euler Equations*:

$$\begin{aligned} &\frac{\partial \rho}{\partial t} + \operatorname{div}(\vec{m}) = 0, \\ &\frac{\partial \vec{m}}{\partial t} + \operatorname{div}\left(\frac{\vec{m} \otimes \vec{m}}{\rho}\right) + M^{-2} \nabla p(\rho) = 0. \end{aligned} \tag{1.2}$$

How good are such zero-viscosity approximations? This is an important current topic of mathematical research in fluid mechanics which we discuss in §§2 and 3 below.

Besides their obvious importance in describing fluid flow, the equations in (1.1), (1.2) are the primary example of a general structure useful for application to many other systems of equations describing a wide variety of complex physical phenomena. The equations in (1.1) and (1.2) are prototypical examples of $m \times m$ systems of conservation laws in N space variables with the form,

$$\frac{\partial \vec{u}}{\partial t} + \sum_{j=1}^{N} \frac{\partial}{\partial x_j} F_j(\vec{u}) = \nu \sum_{j=1}^{N} \frac{\partial}{\partial x_j} (D_j(\nabla \vec{u})). \tag{1.3}$$

Here $\nu > 0$ is a diffusion coefficient and typically satisfies $\nu \ll 1$ in applications. Invoking the zero-diffusion approximation by setting $\nu = 0$, one

obtains the system

$$\frac{\partial \vec{u}}{\partial t} + \sum_{j=1}^{N} \frac{\partial}{\partial x_j} F_j(\vec{u}) = 0. \tag{1.4}$$

Here for $1 \leq j \leq N$, $F_j(\vec{u})$ and $D_j(\nabla \vec{u})$ are given nonlinear mappings from R^m and R^{m^2} respectively to R^m. A partial list of other physical problems besides fluid flow modeled by such systems of equations includes nonlinear elasticity, magneto-fluid dynamics, combustion, super fluids, secondary oil recovery and the equations for meteorology among others. Thus, a systematic mathematical approach to understanding properties of solutions of the equations of fluid flow as a special case of the more general systems in (1.3), (1.4) contributes to increased potential understanding for a wide variety of diverse physical phenomena. Such an approach to (1.3), (1.4) emphasizing the common mathematical structure of the important physical examples has been pioneered by Friedrichs and P. Lax [**4**, **5**]. I illustrate this general approach next and apply it to the equations of fluid flow.

(B) *Nonlinear sound waves and vorticity waves.* I concentrate on the inviscid equations in (1.2) and (1.4) for the remainder of this section. Any constant vector $u_0 \in R^m$ is a special solution of (1.4). Consider perturbed smooth solutions with the form $u^\varepsilon = u_0 + \varepsilon u' + O(\varepsilon^2)$. Substituting this form into (1.4) and collecting the leading power in ε has the consequence that $u'(x, t)$ satisfies the linearized equation,

$$\begin{gathered} u'_t + \sum_{j=1}^{N} A_j(u_0) u'_{x_j} = 0, \qquad x \in R^N, \ t > 0, \\ u'(x, 0) = u_0(x), \end{gathered} \tag{1.5}$$

where $A_j(u) = \partial F_j / \partial u$ are the $m \times m$ Jacobian matrices of F_j and $x = (x_1, \ldots, x_N)$. A minimum requirement on the system in (1.4) is that the problem in (1.5) is well-posed, i.e., solutions exist for reasonable initial data and small changes in the initial data lead to small changes in the solution. This condition is satisfied provided that for every unit direction $\vec{n} = (n_1, \ldots, n_N)$, the $m \times m$ matrix $A(\vec{n}) = \sum_{j=1}^{N} A_j n_j$ has m real eigenvalues and complete eigenvectors; thus there are m real numbers $\{\lambda_j\}_{j=1}^m$ and corresponding nonzero vectors $\{r_j\}_{j=1}^m$ with

$$A(\vec{n}) r_j = \lambda_j r_j, \quad 1 \leq j \leq m. \tag{1.6}$$

In general I assume that r_j is a smooth function of $\vec{n}$. An immediate consequence of (1.6) is that the linearized equation in (1.5) has exact plane wave solutions,

$$u' = \sigma(x \cdot \vec{n} - \lambda_j t) r_j \tag{1.7}$$

for any j with $1 \leq j \leq m$ with $\sigma(s)$ an arbitrary smooth function. For this reason, the eigenvalues $\{\lambda_j\}_{j=1}^m$ are called the wave speeds.

For the equations of fluid flow in (1.2) it is extremely easy to guess the nature of the wave speeds. During a lecture in a relatively still room, the fluid remains still but the *lecturer is heard* through the *propagation of sound waves* in the fluid. On the other hand, a windmill generates swirling of the air without producing much noise; this generation of *swirling* is the *propagation of vorticity waves* in the fluid. Thus, physical intuition leads one to expect that for fluid flow the wave speeds in (1.6) should represent the propagation of sound waves and vorticity waves. This intuition is confirmed through the following fact:

PROPOSITION. *For a given constant state* $(\rho_0, \vec{v}_0)$, $\vec{v}_0 \in R^N$, *there are always* $N+1$ *real wave speeds at* $(\rho_0, \vec{v}_0)$ *for the system in* (1.2) *provided that the nonlinear function* $p(\rho)$ *satisfies* $\frac{dp}{d\rho} > 0$. *Two of the wave speeds,* $\lambda_\pm$, *associated with sound waves, are given by*

$$\lambda_\pm = v_0 \cdot \vec{n} \pm M^{-1} C_0, \tag{1.8A}$$

where $C_0 = (\frac{dp}{d\rho}(\rho_0))^{1/2}$. *The other* $N-1$ *wave speeds, associated with fluid swirling, are the vorticity waves which move with the fluid and have the speed*

$$\lambda_0 = v_0 \cdot \vec{n}. \tag{1.8B}$$

Next I explain the meaning of the constant M, the Mach number. This number represents the ratio of a typical representative fluid velocity magnitude, V, to the typical representative sound speed, C, for the class of fluid flows under consideration, i.e.,

$$M = V/C. \tag{1.9}$$

The Mach number provides a nondimensional reference for the strength of the fluid velocity versus the speed of sound. The air in the wake of an auto moving at 20 m.p.h. satisfies $M \ll 1$ while for a commercial flight on a jumbo jet, M satisfies $M \approx 1$.

Next, I generalize the exact solutions in (1.7) for the linear problem in (1.5) to the nonlinear problem in (1.4) (see [3] for the details). I replace the straight line σr_k in (1.7) by the curve $\sigma \mapsto U(\sigma)$ mapping R^1 to R^m. I also replace the linear argument of σ with the more general form $\sigma(x \cdot \vec{n}, t)$ and seek solutions of (1.4) with the special form

$$u = U(\sigma(x \cdot \vec{n}, t)). \tag{1.10}$$

Such solutions are called nonlinear simple waves. The reader readily verifies that $U(\sigma(x \cdot \vec{n}, t))$ is a solution of (1.4) provided that

(1.11A) the function $U(\sigma)$ satisfies the nonlinear O.D.E. $U_\sigma = r_k(U(\sigma))$ for some k;

(1.11B) with $\lambda_k(\sigma) = \lambda_k(U(\sigma))$, $\sigma(y, t)$ satisfies the scalar nonlinear equation $\sigma_t + \lambda_k(\sigma)\sigma_y = 0$.

In most physical examples including the equations of fluid flow, the nonlinear O.D.E. in (1.11A) can be integrated explicitly.

THE NONLINEAR BEHAVIOR OF SOUND WAVES. The following Proposition summarizes the nature of these exact solutions for the nonlinear sound waves in fluid flow.

PROPOSITION. *Assume that the nonlinear pressure function* $p(\rho)$ *satisfies the convexity condition* $p_{\tau\tau} > 0$ *with* $\tau = \frac{1}{\rho}$. *Then there are exact solutions of the fluid equations in* (1.2) *given by the recipe in* (1.10) *and* (1.11), *where* $\sigma(y, t)$ *satisfies the much simpler scalar nonlinear equation*

$$\sigma_t + (\tfrac{1}{2}\sigma^2)_y = 0, \qquad \sigma(y, 0) = \sigma_0(y). \tag{1.12}$$

Thus, the simpler equation in (1.12) provides a simplified quantitative model for the propagation of special smooth solutions of (1.2) associated with nonlinear sound waves. The equation in (1.12) is the celebrated inviscid Burgers equation. Next I summarize the well-known properties of both smooth and discontinuous solutions of the inviscid Burgers equation (see [**3, 6**]) and contrast these features with those of linear equations. Since the form in (1.10) yields a solution of (1.2) only as long as σ remains smooth, I rely on the discussion of discontinuous solutions of (1.12) to provide qualitative insight into the nonlinear propagation of sound waves in a fluid—this is a simple example of qualitative-quantitative modelling of complex physical phenomena by much simpler equations.

The linear equation $\sigma_t + c\sigma_y = 0$, $\sigma(y, 0) = \sigma_0(y)$ has the explicit solution $\sigma_0(y - ct)$ and the following properties:

(A) If $\sigma_0(y) \in C_0^\infty$, $\sigma(y, t) \in (C^\infty)$ for all t.

(B) The initial data σ_0 is discontinuous at the point y_0 if and only if $\sigma(y, t)$ is discontinuous at the points $y = y_0 + ct$ along the characteristic curve emanating from y.

In contrast, the solution of the *nonlinear equation* $\sigma_t + (\frac{1}{2}\sigma^2)_y = 0$, $\sigma(y, 0) = \sigma_0(y)$ has the following properties:

(1.13A) For every $\sigma_0(y) \in C_0^\infty$, there is a critical time $T_* > 0$ so that $|\sigma'(y, t)| \nearrow \infty$ as $t \uparrow T_0$; thus, solutions never stay smooth for all time.

(1.13B) For discontinuous initial data with the form

$$\sigma_0(y) = \begin{cases} \sigma_L, & y < 0, \\ \sigma_R, & y \geq 0: \end{cases}$$

CASE I. If $\sigma_L > \sigma_R$, $\sigma(y, t)$ is given by

$$\sigma(y, t) = \begin{cases} \sigma_L, & y < \dfrac{\sigma_L + \sigma_R}{2} t, \\ \sigma_R, & y \geq \dfrac{\sigma_L + \sigma_R}{2} t. \end{cases}$$

Thus these solutions have a propagating discontinuity which does *not* move at characteristic wave speed.

CASE II. If $\sigma_L < \sigma_R$, $\sigma(y, t)$ is given by

$$\sigma(y, t) = \begin{cases} \sigma_L, & y < \sigma_L t, \\ y/t, & \sigma_L t \leq y \leq \sigma_R t, \\ \sigma_R, & y > \sigma_R t. \end{cases}$$

Thus, a discontinuity in the initial data disappears for all positive times.

The phenomenon in (1.13A) corresponds to the formation of *shock waves* in a fluid through the nonlinear propagation of sound waves (see Chapter 3 of [3]). The results in Case I of (1.13B) indicate that shock waves do not travel at the speed of sound; this is well known experimentally and mathematically (see [2]). Finally, the smooth solutions with discontinuous initial data given in Case II of (1.13B) are called centered *rarefaction waves* in the general theory because such solutions were discovered first for the fluid equations by Riemann and correspond physically to rarefaction of the gas, i.e., the density of the gas drops by following the gas particles through such a wave. None of the above features occur in linear equations as illustrated by the simple example described above.

NONLINEAR VORTICITY WAVES. Next I apply the construction in (1.10), (1.11) to the wave speeds $\lambda_0 = v_0 \cdot n$ associated with vorticity. For simplicity I consider two space dimensions and $\vec{n} = (1, 0)$. The construction in (1.10) yields exact solutions of the fluid equations with the form

$$\rho = \rho_0, \qquad \vec{v} = {}^t(0, v_2(x_1)). \tag{1.14}$$

These nonlinear vorticity waves are shear layers; the velocity points along the x_2-axis but remains a function of the perpendicular variable, x_1. Such solutions involve only motion of the fluid and no propagation of sound. Furthermore these exact solutions are *incompressible* because the velocity in (1.14) satisfies $\operatorname{div} \vec{v} = 0$. These solutions have *nonzero vorticity* which is defined by $\vec{w} = \operatorname{curl} \vec{v}$ because

$$\operatorname{curl} \vec{v} = -\frac{\partial v_2}{\partial x_1} \neq 0.$$

The propagation and amplification of vorticity produce the dramatic effects of turbulence (see §3).

2. Physical phenomena and mathematical theory for nonlinear sound waves: Recent progress and future directions. Here I describe the current developments in four interesting research areas involving the behavior of nonlinear

sound waves. The first two areas discussed involve rigorous mathematical analysis, while the third involves a combination of rigorous analysis, quantitative asymptotic modelling, and small scale numerical computation. In the fourth topic I describe some of the new insights into the multi-dimensional interaction of nonlinear sound waves which have been produced through recent ingenious large scale numerical simulation. I end this section with some brief speculation on an interdisciplinary attack mingling the four tools in (0.1) which might explain the observed phenomena in the last topic.

(A) *The zero diffusion approximation: the mathematical theory of conservation laws in a single space variable.* Before discussing the specific nature of results in this problem for the equations of fluid flow, I define the basic mathematical issues for a general system in a single space variable (where the mathematical issues are already very difficult!). Thus, I consider solutions u^ν of the $m \times m$ system of equations

$$u^\nu_t + F(u^\nu)_x = \nu(D(u^\nu_x))_x, \qquad t > 0, \ x \in R^1, \tag{2.1A}$$

with given initial data

$$u^\nu(x, 0) = u_0(x), \tag{2.1B}$$

and the corresponding solution of the formal zero diffusion limit with the same initial data

$$\begin{aligned} u_t + F(u)_x &= 0, \qquad t > 0, \ x \in R^1, \\ u(x, 0) &= u_0(x). \end{aligned} \tag{2.2}$$

The structure in (1.6) is assumed so that (2.2) is a nonlinear hyperbolic equation. As explained above (1.2) for the equations of compressible flow, in most problems of physical interest, the diffusion coefficient satisfies $\nu \ll 1$. From the physical point of view, one would like to avoid a detailed assessment of the microscopic effects of diffusion since this is very difficult to achieve both theoretically and experimentally. Thus, the basic *physical issue motivating the mathematical problem of the zero diffusion limit* is the following:

(2.3) Given reasonable initial data $u_0(x)$, find a suitable solution $u(x, t)$ of the system of nonlinear hyperbolic equations in (2.2) so that $u(x, t)$ automatically includes the macroscopic effects of diffusion in $u^\nu(x, t)$, i.e., so that $u^\nu(x, t)$ converges to $u(x, t)$ as $\nu \to 0$ in a suitable sense.

For *smooth* bounded initial data $u_0(x)$, it is not difficult to prove that $u^\nu(x, t) \to u(x, t)$ as $\nu \to 0$ *for* any *time interval* $[0, T_*]$ *such that* the solution $u(x, t)$ *stays smooth* on $[0, T_*]$. S. Klainerman gave an extremely elegant but unpublished proof of this fact several years ago under natural structural assumptions on the diffusion matrix D in (2.1) (private communication) but the author does not know a detailed published reference. However, subtlety in this problem arises because solutions of (2.2) with smooth

initial data typically become discontinuous in finite time (see (1.13A)), [6], and Chapter 3 of [3]); thus, one is naturally forced to deal with *bounded discontinuous solutions which satisfy* (2.2) *in the sense of distributions*, i.e.,

$$\iint (\phi_t \cdot u + \phi_x F(u))\, dx\, dt = 0 \tag{2.4}$$

for all smooth vector-valued test functions $\phi = (\phi_1, \ldots, \phi_m)$ with $\phi_j \in C_0^\infty(R^1 \times (0, \infty))$. With this difficulty, one might as well consider bounded discontinuous initial data, u_0, at the outset. The simplest initial data of this sort for the system in (2.2) are *Riemann* initial data, i.e.,

$$u_0(x) = \begin{cases} u_L, & x < 0, \\ u_R, & x > 0, \end{cases} \tag{2.5}$$

where u_L, $u_R \in R^m$ are two prescribed constants; these data are named after Riemann because he was the first to study this problem for the equations of fluid flow. For example, suppose u_L, u_R are two constant vectors which satisfy the nonlinear algebraic equation (the Rankine-Hugoniot conditions)

$$-s(u_L - u_R) + F(u_L) - F(u_R) = 0. \tag{2.6}$$

Then a weak solution of (2.2) (in the sense of (2.4)) with the initial data in (2.5) is given by

$$u(x, t) = \begin{cases} u_L, & x \le st, \\ u_R, & x > st, \end{cases} \tag{2.7}$$

with the nonlinear wave speed s determined from (2.6). I return to this special problem in the next paragraph. In pioneering work, Lax [4] showed how to get solutions of the Riemann problem for general constants u_L, u_R provided $|u_L - u_R|$ was suitably small; furthermore, this solution was unique in a suitable class of centered-wave solutions provided that certain geometric shock inequalities introduced by Lax were satisfied (pp. 133–137 of [3] contain a detailed rigorous discussion for the motivation behind Lax's shock inequalities). In a brilliant paper which strongly influenced developments in the field for many years, Glimm [7] used Lax's solutions of the Riemann problem as building blocks and established the existence for all $t > 0$ of discontinuous solutions of (2.2) provided that the initial data u_0 had both small amplitude and small total variation (see the book by Smoller [8] for the details of this work and other related developments). The additional geometric structure and large time behavior of solutions of (2.2) constructed through Glimm's method has been elucidated by important further work of Glimm-Lax [9], DiPerna, Liu, and Dafermos among others (see the references in [10, 11]; the article by Dafermos is especially recommended by the author as an introduction to the topics discussed in this subsection). Glimm's theoretical method of existence has also led to interesting new numerical methods (see Chorin [12]). This discussion fills in some background on existence of discontinuous solutions of (2.2).

I return to the special discontinuous initial data satisfying (2.6) and ask whether the weak solution in (2.7) arises as the zero diffusion limit of u^ν as $\nu \to 0$. For appropriate initial data for (2.1) with ν-dependence, this reduces to an interesting question for nonlinear O.D.E.'s which I develop next. It is natural to attempt to build solutions of (2.1) in the form of travelling waves

$$u^\nu(x, t) = U\left(\frac{x - st}{\nu}\right) \tag{2.8A}$$

with

$$\lim_{\xi \to -\infty} U(\xi) = u_L, \qquad \lim_{\xi \to +\infty} U(\xi) = u_R. \tag{2.8B}$$

Clearly, when such a solution exists, $u^\nu(x, t)$ converges to the solution $u(x, t)$ in (2.7) as $\nu \to 0$. The existence of solutions of this sort which solve the zero diffusion limit in (2.3) in a special sense for these special initial data is called the problem of diffusive *shock layers.* This is an extremely important prototype problem because at points of discontinuity, general weak solutions of (2.2) locally look like the solution in (2.7) (see **[10]**). Of course, the advantage in studying (2.8) is that $U(\xi)$ satisfies the simpler $m \times m$ system of nonlinear O.D.E.'s

$$D(U'(\xi)) = F(U(\xi)) - sU(\xi) + C_0 \tag{2.9A}$$

with the constant C_0 given by

$$C_0 = -(F(u_L) - su_L) = -(F(u_R) - su_R). \tag{2.9B}$$

Both u_L and u_R are critical points of the O.D.E. in (2.9) and the existence of shock layers amounts to proving that there is an orbit defined by $U(\xi)$ connecting the critical point u_L with the critical point u_R. As I mentioned earlier in the discussion below (1.1), the full equations of fluid flow include changes in total energy besides the equations for mass and momentum (see **[2, 3]**). As in (1.1) there is no diffusion of mass but diffusion of momentum through viscosity and dissipation of energy through both the effect of viscosity and heat conduction. Beginning around 1910, there has been an enormous interest among physicists and engineers in finding solutions of the shock layer equations in (2.9) for fluid flow and various special solutions were discovered for special ratios of viscosity and heat conduction. Mathematically, shock layers for the full equations of fluid flow reduce to questions regarding 2×2 autonomous systems of O.D.E.s which are amenable to phase portrait techniques. H. Weyl **[13]** contributed to this problem and Gilbarg **[14]** gave the complete solution for generalized ideal gases; in very recent work Pego **[15]** has generalized Gilbarg's results for general equations of state and has provided counter-examples for nonconvex equations of state where *shock layers do not exist if heat conduction dominates viscosity.* Similar results are extremely easy to obtain for the isentropic gas dynamic equations in (1.1),

(1.2) so I sketch the construction below. The equations in (1.1) in a single space dimension are given by

$$\begin{aligned} &\frac{\partial \rho}{\partial t} + \frac{\partial}{\partial x}(\rho v) = 0, \\ &\frac{\partial \rho v}{\partial t} + \frac{\partial}{\partial x}(\rho v^2 + p(\rho)) = \nu \frac{\partial^2 v}{\partial x^2}. \end{aligned} \tag{2.10}$$

The jump conditions in (2.6) in this special case are given by

$$\rho_L(v_L - s) = \rho_R(v_R - s) \equiv m, \qquad m^2 = -\frac{p(\rho_L) - p(\rho_R)}{\tau_L - \tau_R}, \tag{2.11}$$

where $\tau = \frac{1}{\rho}$ is the specific volume and m is a constant, the mass flux. Because there is no diffusion of mass in (2.10), the shock layer solution in (2.9), $u(\xi) = {}^t(\rho(\xi), v(\xi))$, is determined by the solution of the scalar nonlinear O.D.E. for $\tau(\xi)$,

$$\tau'(\xi) = -\frac{1}{m}[m^2(\tau - \tau_L) + p(\tau) - p(\tau_L)]. \tag{2.12}$$

If the mass flux m satisfies $m > 0$, then the fluid velocity satisfies $v_L > s$ and $v_R > s$ so that the fluid particles which move at speed v cross the wave front from the left to the right; similar remarks apply for $m < 0$. By direct quadrature of (2.12), it is easy to prove the following

PROPOSITION. *Consider (isentropic) fluid flow with an equation of state, $p(\tau)$, satisfying the convexity condition $p_{\tau\tau} > 0$ with $\tau = \frac{1}{\rho}$. Consider a weak solution of* (1.2) *defined through* (2.6), (2.7), *and* (2.11). *If $m > 0$ (< 0) a shock layer exists if and only if $\rho_R > \rho_L$ $(\rho_L > \rho_R)$. Thus, shock layers exist at a speed s if and only if the fluid is compressed (the density increases) as fluid particles cross the front.*

The implication of this Proposition for weak solutions of (2.2) is very interesting; there are many weak solutions of (2.2) which are not the zero diffusion limit of solutions of (2.1). For fluid flow, general solutions of (1.2) which satisfy the criterion of being compressive at their discontinuities for convex equations of state are called *entropy solutions* because in the complete equations of fluid flow including entropy, they correspond to weak solutions with increases in entropy in agreement with the second law of thermodynamics. For general equations in (2.1), necessary and sufficient algebraic conditions to guarantee a shock layer in the case that $|u_L - u_R|$ is small have been developed recently by Pego and the author [**16**]; the existence of shock layers when $|u_L - u_R|$ is not small often requires topological methods (see [**8**]).

The existence of shock layers provides intuition but does not even solve the problem of the zero diffusion limit in (2.1)–(2.3) for the special solution in (2.7) satisfying the entropy condition because the initial data defined by (2.8A) changes with ν. To resolve this difficulty, one needs to assess the

nonlinear stability of the shock layer. In recent important work, T. P. Liu has succeeded in doing this both for the equations of fluid flow [**17**] and in general [**18**]. Liu has discovered a number of remarkable new diffusion waves in his rigorous analysis of the limit. Liu's work builds on earlier results of Goodman [**19**] utilizing energy methods under additional assumptions which guaranteed that such diffusion waves are suppressed. Very recently, Liu and Hoff [**20**] have completed the analysis of the quantitative behavior of the zero diffusion limit for discontinuous shock data while Liu and collaborators (personal communication) have rigorously analyzed the zero diffusion limit for piecewise constant rarefaction data in (2.5) where completely different phenomena occur (see (1.13B) for rarefaction data in a simpler problem). It is quite likely that Liu and coworkers will understand the detailed nature of the zero diffusion approximation for general Riemann data in (2.5) in a rigorous constructive fashion in the next few years.

A completely different attack on the question of the zero diffusion approximation is to take the smooth solutions of (2.1), obtain suitable estimates *independent of* ν, and pass to the limit to *construct solutions* of (2.2) automatically satisfying (2.3). In 1951, E. Hopf and Cole independently succeeded in doing this for the model scalar equation

$$u_t^\nu + (\tfrac{1}{2}(u^\nu)^2)_x = \nu u_{xx}^\nu$$

through explicit solution; a general approach for scalar laws utilizing the maximum principle and total variation estimates was developed by Lax, Oleinik, and Kruskov among others (see the bibliography in [**6**, **8**, **11**]). However, for $m \times m$ systems with $m > 1$, it is very difficult to obtain similar a priori estimates which are uniform in viscosity parameters. In 1978, L. Tartar [**21**] introduced a bold new program involving weak convergence and a tool developed by Tartar and Murat [**22**], compensated compactness, which relied on only the obvious uniform bound estimates for u^ν without the harder a priori estimates for derivatives; furthermore, Tartar [**21**] succeeded in giving a new proof of convergence for scalar laws by these methods utilizing the weak topology. Through an extremely novel use and generalization of Lax's entropy pairs, DiPerna [**23**] succeeded in extending Tartar's program to 2×2 systems; in this fashion, DiPerna [**24**] obtained a new existence theorem for the isentropic gas equations in (2.2) in a single space dimension with general large initial data by taking the zero diffusion limit directly.

I end this subsection with two open problems for the mathematical theory of fluid flow in a single space variable. Both problems involve the full 3×3 system of equations involving conservation of mass, momentum, and total energy.

PROBLEM 1. Can the ideas of Tartar and DiPerna be combined with other estimates to study the zero diffusion limit for the 3×3 system of equations for fluid flow?

Another important problem which I have not mentioned is the uniqueness

of weak solutions of (2.2) which satisfy the *entropy* condition (see the above Proposition and [**6, 11**]). In an interesting paper, DiPerna [**25**] has proved the uniqueness of solutions of the Riemann problem in (2.5) within all solutions satisfying the entropy condition provided $m = 2$. DiPerna's argument makes essential use of the condition $m = 2$. A solution of the following problem would be very interesting and seems accessible.

PROBLEM 2. For the 3×3 system of conservation laws given by the equations of compressible fluid flow, prove the uniqueness of solutions of the Riemann problem in the class of bounded functions with bounded variation which are weak solutions satisfying the entropy condition of P. Lax (in [**5, 25**]) for this system. Find conditions on the equation of state and size of the initial data which guarantee this uniqueness theorem.

(B) *Structure and stability of wave patterns in several space variables.* We regard the fluid equations in (1.2) as the prototypical example for general $m \times m$ systems of conservation laws in N space variables with the form

$$u_t + \sum_{j=1}^{N} (F_j(u))_{x_j} = 0 \tag{2.13A}$$

and initial data

$$u(x, 0) = u_0(x). \tag{2.13B}$$

One striking difference between hyperbolic systems in one and several space variables regards the domain of dependence: the solution at a given point of the linearized equations in (1.5) with $N = 1$ is determined by the initial data at a finite number of points; in several space variables, this domain of dependence is much larger and includes an entire cone of initial points. Thus, there are the possibilities for more complex nontrivial interaction of nonlinear sound waves coming from many different directions in multi-D. That such complexity occurs in fluid flows is a documented experimental fact. In particular solutions do not obey simple a priori maximum norm estimates because waves can focus; furthermore, no plentiful simple class of exact solutions such as Lax's solution of the Riemann problem in a single space variable have been found for the fluid equations in (1.2) in several space variables. Nevertheless, solutions of these equations are computed with rather high reliability through numerical methods (see the discussion in §2(D) and §4).

With all of the additional theoretical difficulties for systems in N space variables with $N \geq 2$, the mathematical theory of short-time existence and stability of solutions of (2.13) with special discontinuous initial data has been the main focus of research. The goal of this work is to elucidate the role of inherently multi-dimensional wave interactions in the stability of basic nonlinear wave patterns. The author studied the short-time existence and stability of shock fronts in multi-D (see [**26, 27**], and Chapter 4 of [**3**] for a leisurely introduction). Metevier [**28**] has studied the short-time interaction of two multi-D

shock fronts and recently Alinhac [29] has proved the short-time existence and stability of smooth rarefaction fronts (see (1.13B)) emanating from appropriate piecewise discontinuous initial data. In addition, Harabetian [30] has proved the short-time existence of multi-dimensional curved Riemann problems for piecewise analytic initial data through nonlinear Cauchy-Kowaleski theorems; however, these last results provide no insight into the correct geometric conditions which guarantee the multi-dimensional structural stability of these nonlinear wave patterns. This last comment will become more evident to the reader if he remembers that the Cauchy-Kowaleski theorem can be used to solve the initial value problem for the Laplace equation with real analytic initial data; nevertheless, this initial value problem is clearly ill-posed and cannot be solved for any other smooth initial data which is not real analytic. The techniques involved in all these theorems except the work in [30] require sophisticated ideas from the theory of hyperbolic mixed problems, pseudo-differential operators to obtain stability estimates, and complicated nonlinear iteration schemes. Several open problems for systems of conservation laws in several space variables are discussed at the end of Chapters 3 and 4 of [3].

Here I would like to discuss a new approach to the existence of shock fronts due to E. Thomann and the author [31] which provides a rigorous geometric picture of multi-dimensional shock propagation for an interesting class of systems of conservation laws which arise as second-order wave equations. The prototypical example of a second-order wave equation arises in fluid mechanics in the following fashion: For smooth solutions, the compressible fluid equations in (1.2) can be rewritten in the form

$$\begin{aligned} &\rho_t + \operatorname{div}(\rho\vec{v}) = 0, \\ &\vec{v}_t + (\vec{v}\cdot\nabla)\vec{v} + \nabla h(\rho) = 0, \end{aligned} \tag{2.14}$$

where $h(\rho)$ is determined within a constant by the equation

$$h'(\rho) = \frac{p'(\rho)}{\rho} > 0 \tag{2.15}$$

and $v\cdot\nabla = \sum_{j=1}^{N} v_j \frac{\partial}{\partial x_j}$. With the restriction to fluid flows so that there is a potential function ϕ with $\vec{v} = \nabla\phi$, the last N equations can be integrated to obtain Bernoulli's law,

$$\phi_t + \tfrac{1}{2}|\nabla\phi|^2 + h(\rho) = 0. \tag{2.16}$$

From (2.15) and (2.16), it follows that the density is given by

$$\rho = h^{-1}(-(\phi + t + \tfrac{1}{2}|\nabla\phi|^2)). \tag{2.17}$$

By substituting (2.17) into the equation for conservation of mass in (2.14), a second-order wave equation for the potential ϕ is obtained with the form

$$\frac{\partial}{\partial t}\mathscr{K}_0(d\phi) + \sum_{j=1}^{N} \frac{\partial}{\partial x_j}\mathscr{K}_j(d\phi) = 0. \tag{2.18}$$

Here $d\phi = (\frac{\partial \phi}{\partial t}, \frac{\partial \phi}{\partial x_1}, \dots, \frac{\partial \phi}{\partial x_N})$ and for fluid flow the nonlinear functions $\mathscr{H}_j$ are given by

$$\begin{aligned} \mathscr{H}_0 &= h^{-1}(-(\phi_t + \tfrac{1}{2}|\nabla\phi|^2)), \\ \mathscr{H}_j &= \frac{\partial \phi}{\partial x_j}\mathscr{H}_0, \qquad 1 \le j \le N. \end{aligned} \tag{2.19}$$

The steady form of the equations in (2.18), (2.19) is often used in computational aerodynamics. Since $\vec{v} = \nabla\phi$ satisfies $\operatorname{curl} \vec{v} = 0$, the corresponding fluid flow is irrotational and no vorticity waves occur in these solutions (see §1); the only effects that remain in (2.18), (2.19) are from the nonlinear sound waves.

I sketch the simplified picture of multi-dimensional geometric shock propagation which is used as a theoretical tool in [31] to obtain a very simple proof for existence of shock fronts for second-order wave equations. This rigorous formulation of geometric shock propagation should have other interesting pure and applied consequences. The jump conditions for a weak solution of (2.18) with piecewise smooth gradients across a space-time hypersurface, S, are given by

$$\sum_{i=0}^{N} \nu_i [H_i]_S = 0, \qquad [\phi]_S = 0, \tag{2.20}$$

where brackets, [ ], denote the jump in a quantity across S and $\vec{\nu} = (\nu_0, \nu_1, \dots, \nu_N)$ is the space-time normal to S. Through the special form of the jump conditions, a partial hodograph transformation is introduced on p. 789 of [31]. The location of the shock front S as time evolves is given locally by the graph

$$x_N = u(t, x_1, \dots, x_{N-1}). \tag{2.21}$$

With $y = (y^0, y^1, \dots, y^N)$ and $x' = (x^1, \dots, x^{N-1})$, the function $u(t, x')$ is determined as the restriction of a function $u(y)$ to the point with $y^N = 0$ and $(y^0, y^1, \dots, y^{N-1}) = (t, x')$. The function $u(y)$ solves the auxiliary nonlinear Neumann problem given by

$$\begin{aligned} &\text{(A)} \quad \sum_{j=0}^{N} \frac{\partial}{\partial y_j} \tilde{H}_j(du) = 0, \quad \text{for } y^0 > 0 \text{ and } y^N > 0, \\ &\text{(B)} \quad G(du) = 0, \quad \text{for } y^N = 0, \\ &\text{(C)} \quad u = f_0, \ \frac{\partial u}{\partial y^0} = f_1, \quad \text{for } y^0 = 0, \ y^N > 0. \end{aligned} \tag{2.22}$$

The functions f_0 and f_1 are determined by the initial data and the explicit form of the equation in (2.22A) and the boundary conditions in (2.22B) is given on p. 790 of [31]. Thus, for second-order wave equations, the geometric location of a shock front is determined by the restriction to the boundary of

the solution of an explicit nonlinear Neumann problem for a second-order hyperbolic equation determined by the initial data. Approximate theories of geometric shock dynamics can be developed through suitable approximations to the mixed problem in (2.22). While complete hodograph transformations are ubiquitous in fluid dynamics (see [2]), the work in [31] seems to be the first application of partial hodograph transformations to hyperbolic equations for fluid flow.

(C) *Nonlinear geometric optics.* With the mathematical complexity of solutions of the equations of fluid flow already evident from the discussion above in §§2(A), (B), it is not surprising that applied mathematicians have developed formal asymptotic methods to build simplified quantitative asymptotic approximations. The most prominent method of this sort for linear hyperbolic equations is geometric optics; here I discuss geometric optics for the nonlinear system of conservation laws,

$$u_t + \sum_{j=\phi}^{N} (F_j(u))_{x_j} = 0, \tag{2.23}$$

with a special emphasis on solutions of the compressible fluid equations in (1.2). I summarize some results below and provide references for a more detailed discussion.

The main idea of geometric optics rests in the observation that at high frequencies, i.e., for short wave lengths, solutions of complicated systems can simplify enormously (see [32] for the linear case). Systematic developments of geometric optics for the nonlinear hyperbolic equations in (1.2) or (2.23) involve the basic assumption:

(2.24) The initial data are a small amplitude perturbation with amplitude ε and high frequency $O(\varepsilon^{-1})$ with $\varepsilon \ll 1$.

I illustrate the expansion of geometric optics for (2.23) in the case of initial data that excite only a single mode of propagation. I consider small amplitude perturbations of a constant state u_0 with the initial data given by

$$u_0 + \varepsilon\sigma_0(x, \tfrac{\phi_0}{\varepsilon}) r_p(\nabla\phi_0), \tag{2.25A}$$

where $r_p(\vec{n})$ is the right eigenvector defined earlier in (1.6) and $\nabla\phi_0 \neq 0$. Of course $\nabla\phi_0$ is not necessarily a unit vector and p is fixed with $1 \leq p \leq m$. It is assumed that $\sigma_0(x, \theta)$ is a function with zero mean, i.e,

$$\lim_{T\to\infty} \frac{1}{2T} \int_{-T}^{T} \sigma_0(x, s)\, ds = 0. \tag{2.25B}$$

Functions $\sigma_0(s)$ which satisfy these assumptions include sums of almost periodic functions and functions of compact support. With these assumptions, one builds formal asymptotic solutions of (2.23) with the form

$$u^{\varepsilon} = u_0 + \varepsilon\sigma(x, t, \tfrac{\phi}{\varepsilon}) r_p(\nabla\phi) + \varepsilon^2 u_2(x, t, \tfrac{\phi}{\varepsilon}). \tag{2.26}$$

In order to have a uniformly valid asymptotic expansion, the correction $u_2(x, t, \theta)$ necessarily must grow sublinearly in θ, i.e.,

$$\lim_{|\theta|\to\infty} |\theta|^{-1}|u_2(x, t, \theta)| = 0. \tag{2.27}$$

The ansatz in (2.26) is substituted into (2.23) and successive equations in powers of ε are developed. In order to solve these successive equations subject to the constraint in (2.27), much simpler equations than (2.23) emerge for the phase function, $\phi(x, t)$, and the amplitude function, $\sigma(x, t, \theta)$. In fact, ϕ solves the familiar *eikonal equation of linear geometric optics* for the pth wave,

$$\phi_t + \lambda_p(\nabla\phi) = 0, \qquad \phi|_{t=0} = \phi_0, \tag{2.28}$$

while the amplitude σ solves a nonlinear transport equation

$$D_p\sigma + b_p(\tfrac{1}{2}\sigma^2)_\theta = 0, \qquad \sigma(x, t, \theta)|_{t=0} = \sigma_0(x, \theta). \tag{2.29}$$

The operator D_p is the linear transport operator of geometric optics given by differentiation along the bicharacteristic rays associated with ϕ. As in linear geometric optics [**32**], D_p has the form

$$D_p = \frac{\partial}{\partial t} + \vec{a}_p \cdot \nabla + c_p \tag{2.30}$$

and $\vec{a}_p(x, t)$, $b_p(x, t)$, $c_p(x, t)$ are determined from ϕ by explicit formulas. Thus, geometric optics for a single wave yields enormous simplification in solutions of (2.23). If the coefficient b_p vanishes identically, $b_p \equiv 0$, as occurs for the vorticity waves in fluid flow, then the equations in (2.28), (2.29) reduce to ordinary geometric optics for linear equations [**32**]. However, if $b_p \neq 0$, as occurs for the nonlinear sound waves in fluid flow, we only need to solve the simpler scalar nonlinear equation in (2.29) to construct asymptotic solutions of (2.23). I remark that under the restriction $b_p \neq 0$, the equation in (2.29) can be solved explicitly through solution of the much simpler inviscid Burgers equation,

$$\sigma_\tau + (\tfrac{1}{2}\sigma^2)_\theta = 0,$$

which was discussed earlier in (1.12), (1.13) so a complete explicit solution of (2.29) is available. The reduction of (2.29) to (2.30) requires three coordinate changes: introduction of bicharacteristic coordinates for ∇_p, rescaling σ by a time dependent factor, and finally renormalizing time suitably (see [**33, 34**]). Such single wave expansions for nonlinear geometric optics were developed in the 1940s and 1950s by Lighthill [**35**] and Whitham [**36**] but a systematic treatment was first presented much later by Choquet-Bruhat [**37**] and recently generalized by Hunter and J. B. Keller [**38**]. A leisurely discussion of the derivation of (2.28), (2.29) as well as the remaining topics to be discussed in this subsection is contained in a paper of the author [**39**].

In geometric optics for linear hyperbolic equations, wave patterns superimpose and geometric optics approximations are given by

$$\sum_{p=1}^{m} \sigma_p(x, t, \tfrac{\phi_p}{\varepsilon}) r_p(\nabla \phi_p),$$

where each mode satisfies the eikonal and transport equations separately. Is this true in the nonlinear case? Do new phenomena appear? Recent research of Hunter, Rosales, and the author **[40, 41, 42]** employing a systematic development of nonlinear geometric optics reveals much more complex phenomena; general almost periodic wave trains do not superimpose but instead interact resonantly. In this situation, the nonlinear eikonal equations in (2.28) remain the same but the different amplitudes $\{\sigma_p\}_{p=1}^{m}$ exchange energy through resonant wave interaction. A general theory for this resonant interaction in several space variables is developed in **[41]** and an application to the equations of compressible fluid flow in (1.2) is presented in §6 of **[41]**. In particular, the resonant nonlinear interaction of small amplitude sound waves with vorticity waves produces additional sound waves which resonantly interact. For solutions of the eikonal equations in (2.28) defined by plane waves, after some elementary changes of variable, the amplitudes of the two sound waves $\sigma^{\pm}(\theta, t)$ satisfy the coupled system of resonant equations,

$$\begin{aligned} &\sigma_t^+ + \frac{1}{2}(\sigma^+)_\theta^2 + \int_0^1 k(\theta - y)\sigma^-(y, t)\, dy = 0, \\ &\sigma_t^- + \frac{1}{2}(\sigma^-)_\theta^2 - \int_0^1 k(-\theta - y)\sigma^+(y, t)\, dy = 0, \end{aligned} \tag{2.31}$$

where σ^+, σ^-, and k are periodic in θ with period one. The kernel k is a constant multiple of the vorticity of an initial high frequency nonlinear shear layer as described earlier in (1.14); as given there, k does not change to leading order in time. Clearly the two nonlinear sound waves do not superimpose as in (2.29) but instead resonantly interact through the vorticity wave which defines the convolution kernel in (2.31). Similar asymptotic equations are valid for the complete 3×3 system of compressible fluid flow in a single space dimension (see **[40]**). The matrix convolution kernel in (2.31) is a skew symmetric operator; thus, it conserves the overall energy of the pair (σ^+, σ^-). A recent paper which combines small scale numerical computation and several exact solutions reveals surprising new phenomena in the solutions of (2.31) through resonant wave interaction **[43]**.

The rigorous theory of geometric optics for compressible flow and the general equations in (2.23) is only just beginning. Diperna and the author **[71]** gave a rigorous justification of geometric optics for appropriate systems including (1.2) in a single space variable for initial data of compact support; for these data of compact support resonances of the type described in (2.31) do not occur. The proofs in **[71]** indicate that there are more subtle nonlinear

mechanisms which guarantee that geometric optics is even better for nonlinear problems with discontinuous data than could be predicted by the formal theory! Several accessible open problems in the rigorous theory of geometric optics are mentioned in §4 of [**39**]. The most important and most difficult involves the rigorous justification of the equations in (2.31) describing resonant wave interaction. Another important problem is the rigorous justification of the single wave expansion in (2.25)–(2.30) in several space variables for initial data so that the solutions of (2.29) became discontinuous.

(D) *Nonlinear diffraction at caustics and boundaries.* I illustrate some of the insight which high quality large scale numerical simulations can contribute by discussing the diffraction of nonlinear sound waves. When a shock wave is incident along an inclined ramp, intuition based on linear theory leads one to guess a solution consisting of the incident wave pattern and a reflected curved wave much like that depicted in Figure 1(a). However, recent large scale numerical simulations by Glaz and Colella [**44**] reveal remarkably complex unexpected wave patterns in the diffraction of shocks by ramps. Besides the expected wave pattern in Figure 1(a), more complex reflected wave patterns such as those in Figure 1(b)–(d) occur for various angles and incident wave strengths. In Figure 1(b), the reflected shock is replaced by three shocks and a vorticity wave—this phenomena is called Mach reflection; in Figure 1(d) two different Mach stem structures of this type occur in the reflected wave. Colella and Glaz have found even more of these complex wave patterns embedded in the reflected wave under different flow conditions and for different equations of state. These complex patterns have practical significance because there are higher pressures associated with the triple shock points. Such kinds of complex reflection have been documented experimentally. Plates 235–238 of Van Dyke's book [**1**] describe a sequence of shadow graphs which display experimental phenomena corresponding to the four cases depicted in Figure 1.

Why bother with large scale numerical simulations when experiments show the same phenomena? There are several reasons. First, large scale simulations display all components of the solution such as density, velocity, pressure, vorticity, etc., simultaneously while an experimentalist works very hard to measure changes in a single physical quantity—density changes are measured in the plates 235–238 of [**1**]. A second reason is the ease with which a numerical analyst can change the properties of the material being studied—the differences for example between air, water, and a complex hydrocarbon typically only involve changing a few parameters in a numerical method; for an experimentalist, changing the material under investigation is a major undertaking often requiring a completely different experimental setup.

A basic theoretical issue is the following outstanding problem: why do such complex patterns form and what are the mechanisms generating these patterns? The advantages of numerical codes in studying different parameters

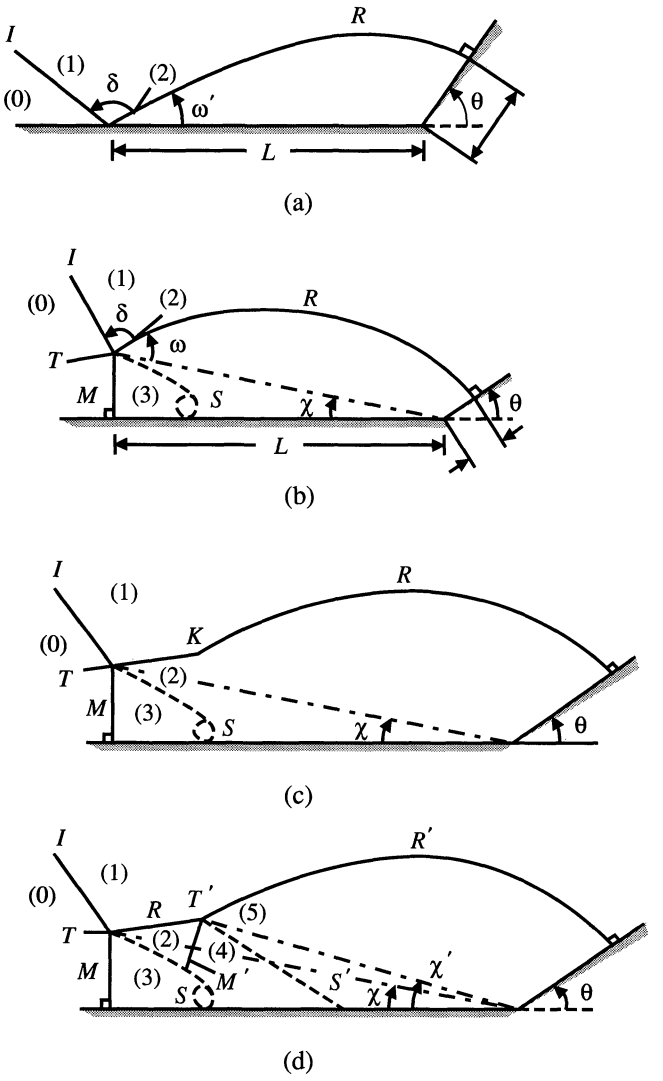

FIGURE 1. Four different types of nonlinear shock diffraction by a ramp. The letter I denotes the incident wave while R denotes the reflected wave.

and displaying all fluid variables, and in gaining a theoretical understanding is enormously important—an example is presented in §4(B) where a new phenomenon in fluid flow involving supersonic vortex sheets has been explained through interaction between large scale computation and theory. For the problems described here, the diffraction effects at shock waves are important; von Neumann recognized many of the possible subtleties and paradoxes in diffraction of nonlinear sound waves (see von Neumann's collected works) but the mechanisms are poorly understood.

I end this section with some brief speculation regarding an approach to explaining the transition from Figure 1(c) to 1(d)—the formation of the second Mach stem. In the vicinity of point K in Figure 1(c), the fluid flow undergoes a transition from subsonic to supersonic, i.e., the local Mach number changes from $M < 1$ to $M > 1$. The steady flow in the vicinity of K can be described by an equation of mixed type with a free surface defined by the reflected shock front. I suspect that the associated linearized equation becomes ill-posed at a critical value of wave strength in a similar fashion as described by Morawetz in her work on perturbed shockless airfoils [**45**]. If this occurs, the complex wave pattern in 1(d) could be explained by incorporating small amplitude nonlinear effects through appropriate geometric optics as described in §2(C).

In other very interesting work in large scale computing on diffraction problems Grove and Glimm [**46**, **47**] have discovered new anomalous wave patterns in shock refraction from an interface between two fluids. Another outstanding theoretical problem is to explain the phenomena observed in these recent calculations.

3. Vorticity waves and turbulence.

(A) *The equations of compressible and incompressible flow.* I recall that the Mach number is the ratio of the typical fluid velocity to the speed of sound. Since the speed of sound in air at room temperature is about 300 meters/sec, most fluid flows in our everyday experience satisfy $M \ll 1$. In the low Mach number limit, $M \downarrow 0$, appropriate solutions of the fluid equations in (1.1) converge to solutions of the *Navier-Stokes equations* of incompressible fluid flow given by

$$\frac{Dv}{Dt} = -\nabla p + \nu \Delta v, \qquad \operatorname{div} v = 0, \tag{3.1}$$

where $v = {}^t(v_1, v_2, v_3)$ is the fluid velocity, $p(x, t)$ is the scalar pressure, and $\frac{D}{Dt} = \frac{\partial}{\partial t} + \sum_{j=1}^{3} v_j \frac{\partial}{\partial x_j}$. The coefficient ν satisfies $\nu \ll 1$ in turbulent regimes and the *equations in* (3.1) with $\nu = 0$ are called the *incompressible Euler equations.*

It is not at all obvious that the solutions of (1.1) converge to those of (3.1) as $M \to 0$ because some of the coefficients in (1.1) are becoming infinite as $M \downarrow 0$. From (1.8) we see that the sound wave speeds in (1.8A) are becoming

infinite while the vorticity wave speeds in (1.8B) remain finite as $M \downarrow 0$. The equations in (3.1) retain only the vorticity waves because the sound waves are moving infinitely fast. The reader can readily verify that the nonlinear vorticity waves in (1.14) are exact solutions of both the equations in (1.2) and the incompressible Euler equations. Rigorous convergence theorems for the incompressible limit due to Ebin [**48**] and Klainerman and the author [**49**, **50**] are of recent vintage even though the folklore of the limit has been understood for over a century (see Chapter 2 of [**3**] for a discussion of the formal limit). Ordinary turbulence occurs in solutions of (3.1) with $\nu \ll 1$, thus vorticity waves are important in turbulence for $M \ll 1$ but sound waves are not.

(B) *An outstanding open problem*: *Breakdown for the* 3-*D Euler equations.* Given the fact that the equation in (3.1) only involves the propagation of vorticity waves, it is revealing to write the equations in (3.1) in an equivalent fashion in terms of the vorticity, $\omega = \operatorname{curl} v$. Taking the curl of the equations in (3.1) leads to the equation,

$$\frac{D\omega}{dt} = \mathscr{D}\omega + \nu\Delta\omega, \tag{3.2}$$

where $\mathscr{D}$ is the 3×3 symmetric matrix, the deformation matrix, given by

$$\mathscr{D} = \tfrac{1}{2}(\nabla v + (\nabla v)^T). \tag{3.3}$$

The velocity, v, is determined from the vorticity ω via potential theory from

$$\operatorname{curl} v = \omega, \qquad \operatorname{div} v = 0$$

and the resulting formula can be differentiated to compute $\mathscr{D}$ as a strongly singular integral operator applied to ω. In this fashion (3.2) becomes an evolution equation for the vorticity alone which is equivalent to (3.1). The terms $\frac{D\omega}{Dt}$ and $\nu\Delta\omega$ produce convection and diffusion of vorticity respectfully; neither of these effects amplifies vorticity. However, the term $\mathscr{D}\omega$ on the right-hand side of (3.2) is the "tornado mechanism" which can amplify vorticity enormously. Here is the reasoning: the deformation matrix in (3.3) is a symmetric matrix with zero trace and always has positive eigenvalues provided $\mathscr{D} \neq 0$. If the vorticity roughly aligns with an eigenvector corresponding to a positive eigenvalue, ω increases. It is not difficult to present examples of exact solutions where ω increases. I am somewhat terse here because this material has already been discussed with examples in another paper of the author [**51**].

The outstanding problem regarding breakdown for the 3-D incompressible Euler equations is the following:

(3.4) Are there smooth incompressible velocity fields with finite energy so that the vorticity accumulates so rapidly that the solution of 3-D Euler becomes singular at a finite time?

This is an outstanding unsolved problem which has been attacked through a large number of ingenious numerical approaches (see [51]) which suggest singularity formation but no rigorous examples of smooth solutions with finite energy forming singularities are known. A theorem of Beale, Lato, and the author [52] states that a smooth solution with finite energy becomes singular at a finite time T_* if and only if

$$\int_0^T |\omega(s)|_{L^\infty}\, ds \to \infty \quad \text{as } T \nearrow T_*. \tag{3.5}$$

Here $|\omega(s)|_{L^\infty} = \max_{x \in R^3} |\omega(x, s)|$. This theorem provides a convenient test for checking numerical computations. It is extremely difficult to devise numerical methods to compute solutions with singularities. Is the actual solution blowing up or just the numerical solution? The above theorem suggests that the quantity to monitor in numerical calculations is given on the left-hand side of (3.5). In particular if a numerical method predicts singularity formation but the quantity in (3.5) remains finite, one is guaranteed that the numerical method is creating fictitious singular solutions. Siggia and Shelley/Meiron have independently been using the test in (3.5) in their recent numerical simulations (personal communication). I have mentioned this possibility here as a simple example of rigorous theory providing guidelines for numerical computation. Other comments of the author regarding (3.4) and additional references are found in [51].

Why is (3.4) a fundamental problem in mathematical fluid dynamics? The reason is that most current turbulence theories seem to imply the existence of many singular solutions for 3-D Euler. For example, Kolmogorov's famous theory requires that the dissipation rate ε is constant for small values of ν; this dissipation rate is given by

$$\varepsilon = \nu \overline{\omega^2},$$

where the bar denotes averaging over statistical ensembles of velocity fields. If ε is constant as $\nu \to 0$, clearly $\overline{\omega^2}$ becomes infinite and there should exist plentiful families of singular solutions for 3-D Euler. This reasoning is vague and imprecise but it does motivate the importance of the problem posed in (3.4).

(C) *Current turbulence theories and modern mathematical physics.* This subsection is the shortest of this paper but perhaps the most important for future research developments. This is an exciting time in turbulence theory. Chorin has developed a statistical theory of vorticity in turbulence based on analogies in polymer physics and self-avoiding random walks [53]. V. Yakhot and co-workers [54] have developed a theory of renormalization group turbulence based on analogy with Wilson's renormalization group in critical phenomena. Can these connections between modern physics and turbulent fluids be elucidated and made more precise through an appropriate combination of ideas utilizing all four facets of (0.1)?

4. Examples of the interaction between large scale computing and modern mathematical theory: Vortex sheets in two distinct regimes of fluid motion. Vortex sheets are piecewise smooth exact solutions of the fluid equations in (1.2) characterized by continuity of the pressure and normal velocity but with a discontinuity in the tangential velocity. The vorticity in a vortex sheet, $\operatorname{curl} \vec{v}$, is a distribution given by a Dirac delta measure supported by the curve. A simple example of a vortex sheet is the steady exact solution of (1.2) defined by

$$\begin{pmatrix} \rho \\ v_1 \\ v_2 \end{pmatrix} = \begin{cases} {}^t(\rho_0, 0, V), & x_1 > 0, \\ {}^t(\rho_0, 0, -V), & x_1 < 0, \end{cases} \tag{4.1}$$

with $V > 0$, a constant velocity. This is a weak solution of the fluid equations in (1.2) with the vortex sheet given by the line $x_1 = 0$ and the vorticity, $\operatorname{curl} \vec{v}$, given by

$$\operatorname{curl} \vec{v} = 2V\delta(x_1) \tag{4.2A}$$

with $\delta(x_1)$ the Dirac mass at $x_1 = 0$. The Mach number associated with the vortex subset in (4.1) is given by

$$M = \frac{V}{c(\rho_0)}, \tag{4.2B}$$

where $c^2(\rho_0) = p'(\rho_0)$ defines the speed of sound. In this section, we give examples of the interaction between large scale computing and mathematical theory in studying the evolution of vortex sheets. The mathematical ideas and physical phenomena will be very different depending on the two regimes of motion to be considered as I explain next.

In §4(A), we discuss the evolution of vortex sheets like the one in (4.1) in the regime of low Mach numbers, $M \ll 1$. For $M \ll 1$, as I discussed in §3, it is appropriate to use the equations of incompressible flow without viscosity. Furthermore, like the other vorticity waves in (1.14), the simple exact solutions in (4.1) are also weak solutions of the equations for incompressible flow. Such thin layers of vorticity occur naturally in fluid flows for instance in the trailing wake of airwings and in the piston motion of an internal combustion engine. Plates 76, 145, and 146 from Van Dyke's book [**1**] are experimental photographs of vortex sheets with $M \ll 1$—the vorticity is concentrated in such thin layers with $\nu \ll 1$ that idealizations with $\nu = 0$ and infinitely thin layers are commonly used. Such problems are extremely difficult from both the computational and mathematical point of view for the following reason: for the incompressible limit with $M \ll 1$, the exact solutions in (4.1) are violently unstable—the linearized initial value problem about these exact solutions behaves like the initial value problem for the Laplace equation and is strongly ill-posed [**55**]. The plates 145, 146 from [**1**] give an experimental confirmation of this behavior which is known as nonlinear Kelvin-Helmholtz instability. The numerical computations and mathematical theory in §4(A)

address the incredibly complex phenomena which occur for longer times and for vortex sheet initial data; these data are not typically real analytic in many practical applications.

In §4(B), we discuss the evolution of vortex sheets like the one in (4.1) in a completely different regime where the flow speed V is extremely fast, i.e., the Mach number satisfies $M > 1$ so that these are *supersonic* vortex sheets. There has been increasing applied interest in the structure of perturbed supersonic vortex sheets motivated by both the structure and motion of galactic jets in astrophysics and the possibility of designing space planes which fly at extremely high Mach numbers—the mixing environment for fuel and oxidant involves fluid flows like the one in (4.1) with $M > 1$. It is extremely difficult and expensive to do experiments at such high Mach numbers so a combination of large scale computing and mathematical theory is potentially very useful in understanding fluid phenomena in this regime. In fact, in §4(B) we present a completely new mechanism for the nonlinear instability of supersonic vortex sheets at high Mach numbers—these phenomena occur for Mach numbers satisfying $M > \sqrt{2}$. For $M > \sqrt{2}$ vortex sheets develop nonlinear instability in a completely different fashion than through nonlinear Kelvin-Helmholtz instability. In this regime $M > \sqrt{2}$, small amplitude nonlinear sound waves interact through shock and rarefaction patterns and generate increasing vorticity through resonant wave interaction. In contrast, for vortex sheets with $M \ll 1$, no interaction of sound waves and vorticity can occur in the incompressible limit because the sound waves have been removed (see §3). These new mechanisms of instability have been discovered and understood very recently through a sophisticated combination of numerical experiments and mathematical theory which we summarize briefly in §4(B).

(A) *The nonlinear evolution of vortex sheets for 2-D incompressible flow.* A two-dimensional incompressible velocity field, $v_0(x)$, defines *vortex sheet initial data* provided that there is a piece of a smooth curve C in the plane so that the tangential velocity of $v_0(x)$ jumps across C while the normal velocity for $v_0(x)$ remains continuous. Here, for simplicity, we assume that $v_0(x)$ is a potential flow outside C. Thus, the vorticity $\omega_0 = \operatorname{curl} v_0$ has the following structure:

(4.3A) the vorticity ω_0 is a surface Dirac delta measure supported on C.

Another obvious physical requirement for vortex sheet initial data is that v_0 has locally finite kinetic energy, i.e.,

$$\int_{|x| \le R_0} |v_0|^2 \, dx \le C_{R_0} \quad \text{for any } R_0 > 0. \tag{4.3B}$$

In the remainder of this subsection, when we refer to vortex sheet initial data, we tacitly assume the conditions in (4.3). There is an enormous engineering

and applied mathematics literature on these topics involving both formal asymptotic methods and numerical simulation (see [56]).

First I describe some of the remarkable computational results achieved by R. Krasny [57] recently using computational vortex methods with a regularization parameter δ. The actual motion of the vortex sheet is recovered in the limit $\delta \downarrow 0$. Krasny presents calculations of roll-up vortex sheets without a distinguished sign and the subsequent evolution can be incredibly complex. In the first calculations discussed in [57], Krasny studies the numerical solution for vortex sheet initial data corresponding to an elliptically loaded wing. Figures 7–15 of [57] demonstrate the convergence as $\delta \downarrow 0$ of the regularized algorithm in the vicinity of the tips which roll-up. As further evidence for the validity of his numerical procedure he also compares the numerical solution with Kaden's self-similar spiral; asymptotic arguments predict this solution controls the behavior of the roll-up. The second calculations reported by Krasny have initial data with a vortex sheet strength that changes sign three times. The vortex sheet rolls-up at six different locations and the different pieces of the sheet globally interact like large scale vortices with various signs. Figure 2 on the next page. (Figure 19 from [57]) shows the middle stages of development while Figure 3 see page 379 (Figure 23 from [57]) shows the incredible small scale complexity in the vortex sheet generated by the large scale coherent structures on the sheet which drive their development. Figures 4, 5, and 6 see page 380 (Figure 24 from [57]) give closeup views of the incredibly complex portions of the vortex sheet that develop as time evolves. The "fat" portions from the vortex sheet in Figures 5 and 6 are artifacts of the graphics printing; in fact the vortex sheet has folded in several closely packed strips. These last calculations use the crude value of $\delta = 0.1$—it is difficult to imagine the structure of the solution as $\delta \downarrow 0$. A mathematical framework designed to address such observed complexity is discussed later in this section.

Next I describe another very interesting numerical computation of a perturbed periodic vortex sheet by Shelley and Baker [58]. They approximate the slightly perturbed initial vortex sheet by a layer with mean finite thickness h and uniform vorticity inside with strength $C_0 h^{-1}$, where C_0 is a given constant. These authors consider a sequence of calculations with these initial data as $h \to 0$, i.e., as the uniform sheet gets thinner—this is another regularization procedure for the singular vortex sheet. They resolve the behavior of the inviscid fluid flow with fixed h by a sophisticated interface algorithm which tracks the boundaries. The results of their computations with their smallest value of $h = 0.025$ are presented in Figures 7 and 8 see page 381. The successive times depicted are $t = 0$, 1.5, 2.0, 2.2, and 2.4. One interesting facet of these calculations is the approximate Kirchhoff ellipse which forms by time 2.4 in the roll-up process. An ellipse with the same ratio of major and minor axes was present in all the resolved runs from [58] and has

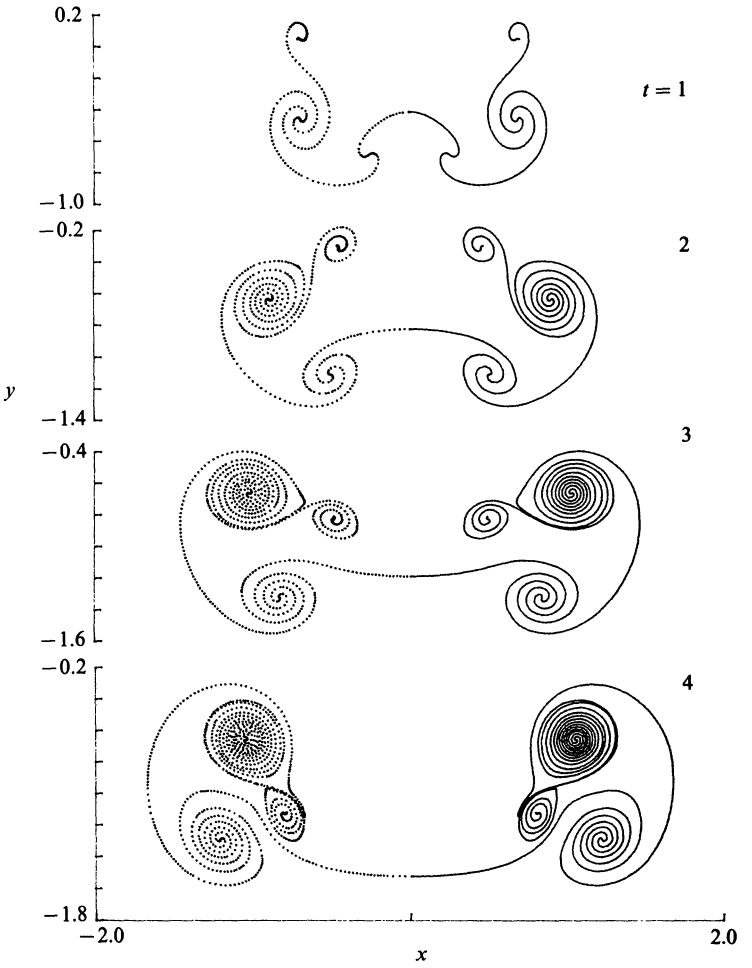

FIGURE 2. The solution plotted over the time interval $1 \leq t \leq 4$ using $\delta = 0.1$ (R. Krasny [57]).*

* Reprinted with the permission of Cambridge University Press. This figure originally appeared in *Computation of vortex sheet roll-up in the Treffitz plane*, by Robert Krasny, Journal of Fluid Mechanics, Cambridge University Press, Cambridge, 1987.

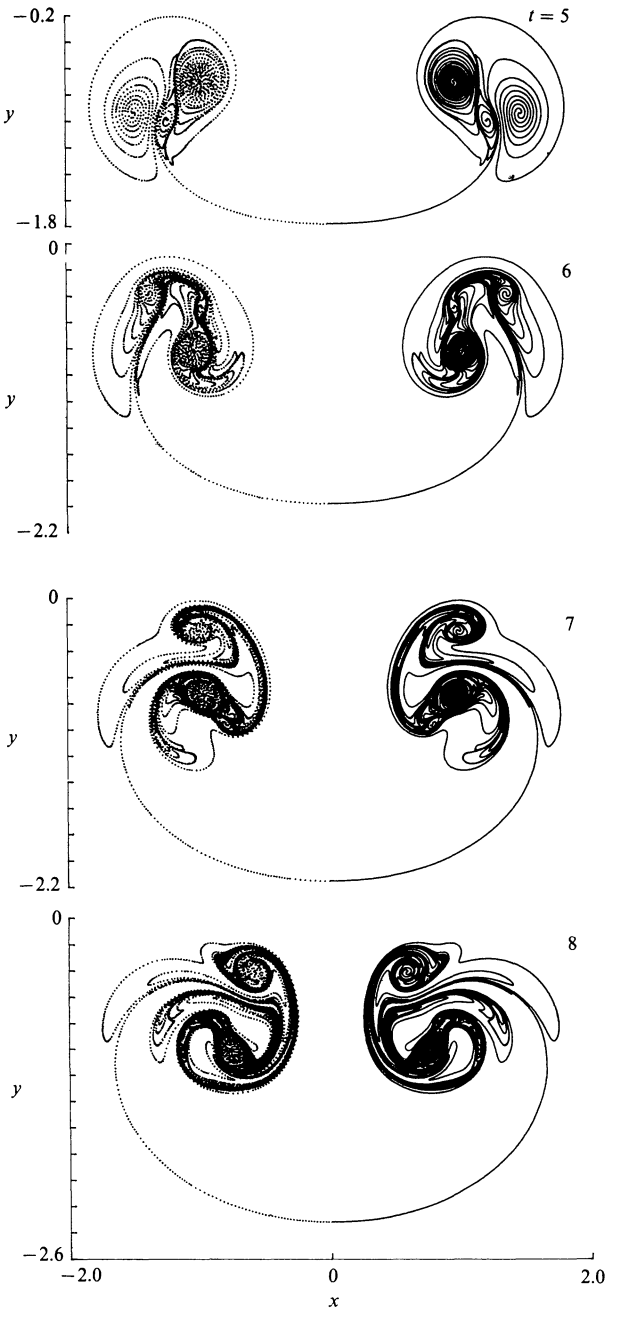

FIGURE 3. Evolution over the time interval $5 \leq t \leq 8$ for $\delta = 0.1$ (R. Krasny [57]).**

** Reprinted with the permission of Cambridge University Press. This figure originally appeared in *Computation of vortex sheet roll-up in the Treffitz plane*, by Robert Krasny, Journal of Fluid Mechanics, Cambridge University Press, Cambridge, 1987.

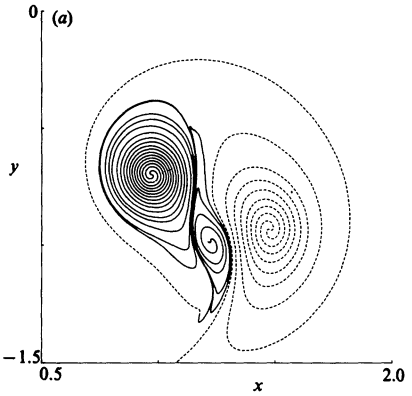

FIGURE 4. Closeup view of the solution at $t = 5$ (R. Krasny [57]). †

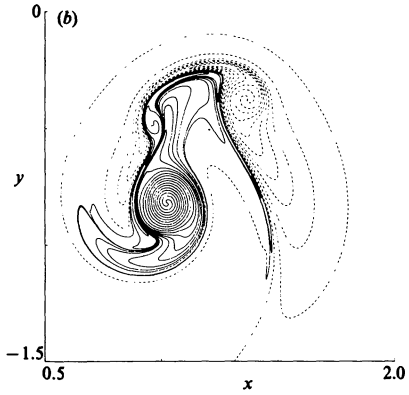

FIGURE 5. Closeup view of the solution at $t = 6$ (R. Krasny [57]). †

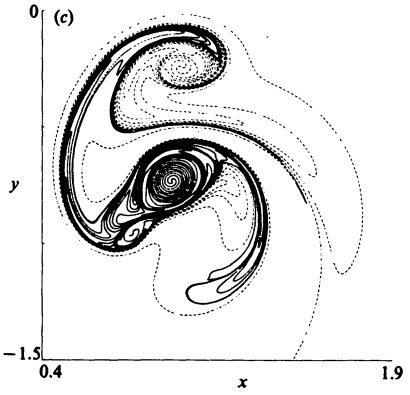

FIGURE 6. Closeup view of the solution at $t = 7$ (R. Krasny [57]). †

† Reprinted with the permission of Cambridge University Press. This figure originally appeared in *Computation of vortex sheet roll-up in the Treffitz plane*, by Robert Krasny, Journal of Fluid Mechanics, Cambridge University Press, Cambridge, 1987.

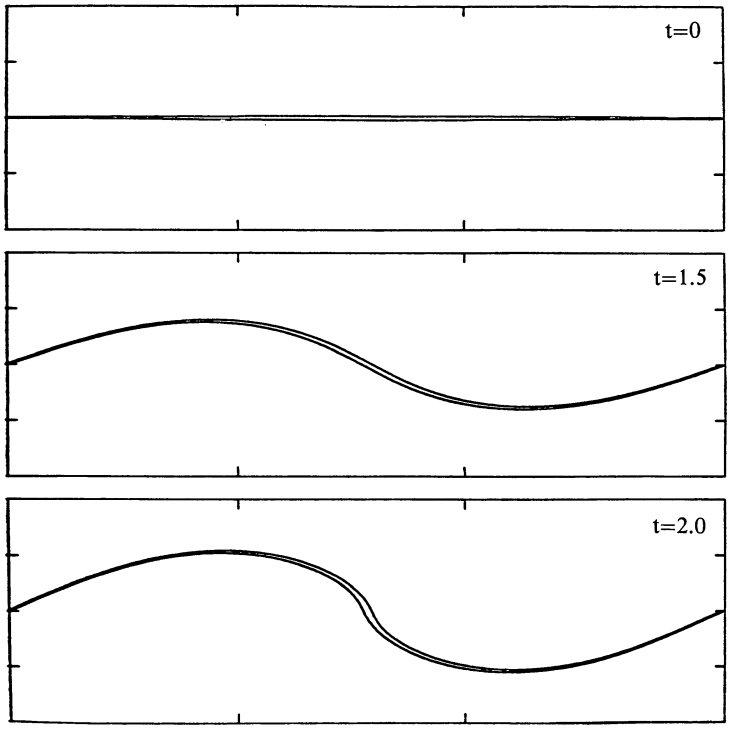

FIGURE 7. The solution at time $t = 0$, 1.5, and 2.0 with $h = 0.025$.[††]

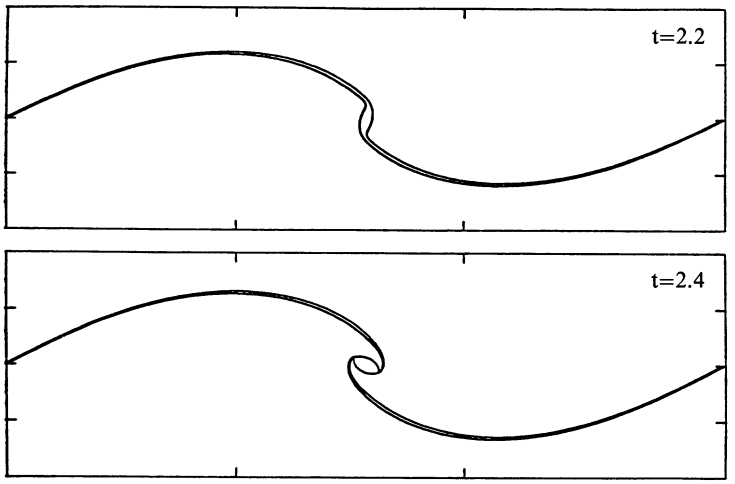

FIGURE 8. The solution at time $t = 2.2$, 2.4 with $h = 0.025$.[††]

[††] Provided by Michael Shelley. More complete results appear in [58].

an area which scales with h as $O(h^{1.6})$ as $h \downarrow 0$. This fact together with the fact that that vorticity has a single sign is an important aspect of these calculations for the mathematical theory which I sketch below.

I briefly describe a program developed in joint work by DiPerna and the author [**59**, **60**, **61**] specifically designed to address the new phenomena that arise in taking limits of suitable approximate solution sequences for 2-D and 3-D Euler. I mostly discuss this theory and its implications for approximate solution sequences for 2-D Euler with vortex sheet initial data and indicate how the above theory provides insight into the trends observed in the calculations of Krasny and Shelley and Baker. A leisurely but more detailed discussion than presented here of the work in [**59**]–[**61**] is presented in another recent paper of the author [**62**].

APPROXIMATE SOLUTION SEQUENCES FOR 2-D EULER WITH VORTEX SHEET INITIAL DATA. I consider an initial incompressible velocity field v_0 in two space dimensions for the evolution of a vortex sheet. Thus I assume that v_0 has the structure (4.3), i.e., the vorticity ω_0 is a surface Dirac delta measure and the velocity v_0 has locally finite kinetic energy. The basic physical problem involved in the evolution of vortex sheets in the high Reynolds number limit is the following:

(4.4) If $v^\nu(x, t)$ is the solution of the Navier-Stokes equations with vortex sheet initial data v_0, does $v^\nu(x, t)$ converge in the high Reynolds number limit as $\nu \to 0$ to a solution of the inviscid 2-D Euler equations? Do new phenomena occur in the limiting process? Do solutions of inviscid 2-D Euler with vortex sheet initial data exist for all time?

I have just described two other ways to generate approximate solution sequences for 2-D Euler with vortex sheet initial data via computational algorithms. The same basic questions described in the first part of (4.4) apply to the two computational regularizations for 2-D Euler just described above. Another important question is the following:

(4.5) Do different regularizations for 2-D Euler with vortex sheet initial data converge to the same answer?

In §1 of [**60**], DiPerna and the author introduce the concept of approximate solution sequence for 2-D Euler. Loosely speaking, we say that v^ε is an approximate solution sequence for 2-D Euler provided that the following three conditions are satisfied:

(1) v^ε is an incompressible velocity field with *local kinetic energy* uniformly bounded independent of ε, i.e.,

$$\max_{0\le t\le T}\int_{|x|\le R}|v^\varepsilon|^2\,dx \le C(R,T)$$

for any R, $T>0$.

(2) The vorticity $\omega^\varepsilon = \operatorname{curl} v^\varepsilon$ satisfies

$$\max_{0\le t\le T}\int |\omega^\varepsilon|\,dx \le C. \tag{4.6}$$

(3) The *sequence of velocity fields* v^ε is *velocity consistent with 2-D Euler*, i.e., for all smooth vector test functions $\phi(x,t)=(\phi_1,\phi_2)$, with bounded support and $\operatorname{div}\phi = 0$, as $\varepsilon\to 0$

$$\iint (\phi_t\cdot v^\varepsilon + \nabla\phi : v^\varepsilon\otimes v^\varepsilon)\,dx\,dt \to 0.$$

Here $v\otimes v=(v_iv_j)$, $\nabla\phi=(\partial\phi_i/\partial x_j)$, and $A\colon B$ denotes the matrix product $\sum_{i,j}a_{ij}b_{ij}$. The estimate in (2) of (4.6) is the natural one for 2-D vortex sheet data (see **[60]**).

I note that for vortex sheet initial data v_0, if 2-D Euler has a solution $v(x,t)$ then this solution is not smooth and would only be a solution in the "weak" distributional sense, i.e., for all smooth ϕ with $\operatorname{div}\phi=0$

$$\iint (\phi_t\cdot v + \nabla\phi : v\otimes v)\,dx\,dt = 0, \tag{4.7}$$
$$\operatorname{div} v = 0 \quad \text{in the sense of distributions.}$$

The equation in the first part of (4.7) arises from writing the 2-D Euler equations in conservation form, multiplying the ϕ, and integrating by parts in a fashion familiar to the reader perhaps from equation (2.4) in hyperbolic shock wave theory. With the natural definition in (4.7), I observe that the condition in (3) of (4.6) is the minimum requirement needed for a sequence of approximate solutions to have any change of converging to a solution of 2-D Euler as $\varepsilon\to 0$. A portion of **[60]** is devoted to a proof of the following important results:

THEOREM. *All three of the regularization processes described above with vortex sheet initial data generate approximate solution sequences for 2-D Euler satisfying the conditions in* (4.6). *For the high Reynolds number limit of the Navier-Stokes equations,* $\nu=\varepsilon$; *for the regularization of Shelley and Baker,* $h=\varepsilon$; *while for the class of computational vortex methods described in* **[60]**, $\varepsilon=\delta$ *with* δ *and* h *suitably linked.*

The complexity observed in the calculations of Krasny indicates that the limits as $\varepsilon\to 0$ of approximate solution sequences can be incredibly complex. Do new phenomena occur in the limiting process for approximate

solution sequences? Examples indicate that the answer is yes. The simplest way to generate examples of approximate solution sequences is to take exact solutions for 2-D Euler satisfying the conditions in (4.6)—of course, (4.6)(3) is trivially satisfied for these sequences. Two examples discussed in **[59, 60]** are generated by utilizing swirling flows given by

$$v = \begin{pmatrix} -x_2 \\ x_1 \end{pmatrix} |x|^{-2} \int_0^{|x|} s\omega(s)\, ds\,, \tag{4.8}$$

where $\omega(r)$ is a radial function. These are well-known exact solutions of 2-D Euler with $\operatorname{curl} v = \omega(r)$.

EXAMPLE 1. Pick a *positive radial vorticity* distribution $\omega \geq 0$ with bounded support and define v^ε to be the scaled exact swirling flow

$$v^\varepsilon = \left(\log \frac{1}{\varepsilon}\right)^{-1/2} \frac{1}{\varepsilon} v\left(\frac{x}{\varepsilon}\right),$$

with v given from ω by (4.8). Then all the assumptions in (4.6) are satisfied.

EXAMPLE 2. Pick a radial *vorticity distribution* with bounded support but *zero total circulation*, i.e., $\int_0^\infty s\omega(s)\, ds = 0$, and define v^ε by

$$v^\varepsilon = \varepsilon^{-1} v\left(\frac{x}{\varepsilon}\right),$$

with v given from ω by (4.8). Then all of the assumptions in (4.6) are satisfied. These exact solutions are called "phantom" vortices in **[60]** because these swirling flows vanish identically outside a circle of radius $O(\varepsilon)$ as $\varepsilon \to 0$ (see **[59, 60]** and the recent paper by Greengard-Thomann **[63]** for more sophisticated examples).

What happens to the limit as $\varepsilon \to 0$ of these exact swirling flows? First, it is easy to see in both examples that

$$v^\varepsilon \rightharpoonup 0 \tag{4.9}$$

although the convergence is weak and certainly not uniform. On the other hand, if we multiply the nonlinear terms $v_i^\varepsilon v_j^\varepsilon$ by a smooth function $\phi(x_1, x_2)$ with bounded support and average,

$$\lim_{\varepsilon \to 0} \int_{R^2} \phi v_i^\varepsilon v_j^\varepsilon = C\phi(0)\delta_{ij}, \qquad C \neq 0, \tag{4.10}$$

where

$$\delta_{ij} = \begin{cases} 1, & i = j \\ 0, & i \neq j. \end{cases}$$

The constant C differs in Example 1 and Example 2 and depends on different averages of the vortex core structure in each of the two different cases. In the language of distributions, (4.10) means that

$$v^\varepsilon \otimes v^\varepsilon \rightharpoonup C \begin{pmatrix} 1 & 0 \\ 0 & 1 \end{pmatrix} \delta(x), \tag{4.11}$$

with $\delta(x)$ the Dirac delta function at the origin. Naively, one might have expected from (4.9) that $v^\varepsilon \otimes v^\varepsilon \rightharpoonup 0$. Instead new phenomena of *concentration* have occurred in the limit. A *finite amount of local kinetic energy* (exactly $2C$) *has been lost in the limit* in these examples *and concentrates on a small set of measure zero*, the origin in R^2. Thus, new phenomena of concentration occur in limits of approximate solution sequences. The concept of measure-valued solution for 2-D Euler is introduced in **[59, 60]** to allow for such potential complexity in the limiting process. This concept of measure-valued solution with concentrations and oscillations was strongly motivated by Tartar's **[21]** earlier use of the Young measure to study oscillations. One important fact proved in **[59, 60]** is the following

THEOREM. *Every approximate solution sequence for 2-D Euler with vortex sheet initial data converges for all time to a measure-valued solution of 2-D Euler. This solution has concentrations but no oscillations.*

I remark that the concept of measure-valued solution guarantees only that the 2-D Euler equations are satisfied in a very weak sense involving expected values of certain probability measures. Nevertheless, this is an extremely flexible concept. Thus, not every measure-valued solution for 2-D Euler is a weak solution as defined in (4.7) although the converse is true. The exact solution sequences from Example 1 and Example 2 generate examples of nontrivial measure-valued solutions (see **[60]**). In fact, the author conjectures that if one takes a limit as $\delta \downarrow 0$ for a sequence of calculations like the one of Krasny depicted in Figures 2–6 with the crude value of $\delta = 0.1$, the following scenario is possible: there is a critical time t_c so that for $t < t_c$ the limit is a weak solution of 2-D Euler in the standard sense of (4.7) while for $t > t_c$ the weak solution bursts into a much more complex measure-valued solution for 2-D Euler. The guess that a measure-valued solution occurs for $t > t_c$ is based not only on the enormous complexity of the evolving vortex sheet for crude $\delta = 0.1$ but also because this complexity occurs as a consequence of the fact that *vorticity of different signs concentrates* in a *small* region of *space* and attempts to cancel in an inviscid flow. The simple Example 2 involving phantom vortices necessarily has vorticity with changing signs; as explained in detail in §1 of **[60]**, much less singular local behavior occurs in the concentrations from Example 2 than in those from Example 1 with a fixed sign of the vorticity. Since the behavior of concentration is less singular when the vorticity changes sign, the changes of developing concentrations are much greater.

Next, through a combination of theory from **[60]** and observed trends in the numerical data, I present strong evidence that in the limit as the thickness $h \to 0$ for the calculations of Shelley and Baker depicted in Figures 7 and 8 with $h = 0.025$, the limit is expected to be an ordinary weak solution of 2-D Euler. The vorticity in this calculation has a distinguished positive sign. Theorem 3.1 of **[60]** contains a criterion to check whether a given

approximate solution sequence converges to a classical weak solution of 2-D Euler; this criterion is especially useful when the vorticity has one sign. For the regularization considered by Shelley and Baker, the far-field condition in (3.5) of [**60**] is readily verified. Thus, for the specific regularization used by Shelley and Baker, Theorem 3.1 from [**60**] has the following special form:

THEOREM. *Assume that the approximate vorticity* ω^ε *has a distinguished sign,* $\omega^\varepsilon(x, t) \geq 0$. *Also assume that*

$$\max_{\substack{x_0 \in R^2 \\ 0 \leq t \leq T}} \int_{|x-x_0| \leq R} \omega^\varepsilon \, dx \leq C \log\left(\frac{1}{R}\right)^\beta \quad \text{for all } R \leq R_0 \tag{4.12}$$

for some fixed constant C *and some* β *with* $\beta > 1$. *Then as* $\varepsilon \to 0$ *the corresponding velocity fields* v^ε *of the approximate solution sequence converge strongly to an ordinary weak solution of 2-D Euler satisfying* (4.6) *for* $0 < t < T$.

Next, I check the criterion in the above theorem according to the computational trends depicted in Figures 7 and 8. We recall that the approximate Kirchhoff ellipse that occurs at time $t = 2.4$ was present in a sequence of three resolved runs with roughly the same ratio of major to minor axes in the ellipse as $h \downarrow 0$ while the area of this ellipse was $O(h^{1.6})$. Since the vorticity has constant strength $O(h^{-1})$ inside the bounding curves, with the information just presented, the maximum value of the ratio of the left- and right-hand sides of (4.12) occurs at $t = 2.4$ at the center of the ellipse for $R \approx h^{0.8}$. Since

$$h^{0.6} \ll (\log(h^{-0.8}))^{-\beta} \quad \text{as } h \downarrow 0,$$

for any $\beta > 1$, the criterion in (4.12) is satisfied and the limit is expected to be a classical weak solution for 2-D Euler.

I mention here that the criterion in (4.12) is almost sharp; the sequence of swirling flows with vorticity of positive sign from Example 1 satisfies an estimate like (4.12) with the value $\beta = 1/2$ but develops concentrations and does not converge strongly. Thus, a criterion such as $\beta > 1$ is needed and almost sharp. When the vorticity locally has a distinguished sign, formal asymptotic methods [**56**] often predict that the left-hand side behaves like $O(h^\alpha)$ with $\alpha > 0$, thus a classical weak solution is predicted by the Theorem in these instances.

I also remark that it is still possible for the limit of an approximate solution sequence to be an ordinary weak solution of 2-D Euler even though concentrations develop and there is a loss of kinetic energy—this possibility is explored in detail in [**61**] with several positive results and is called concentration-cancellation. A more leisurely mathematical discussion is presented in [**62**]. Also, while the author knows of no explicit rigorous examples where a weak solution for 2-D Euler with vortex sheet initial data bursts at a certain time into a measure-valued solution as expected in the $\delta \downarrow 0$ limit

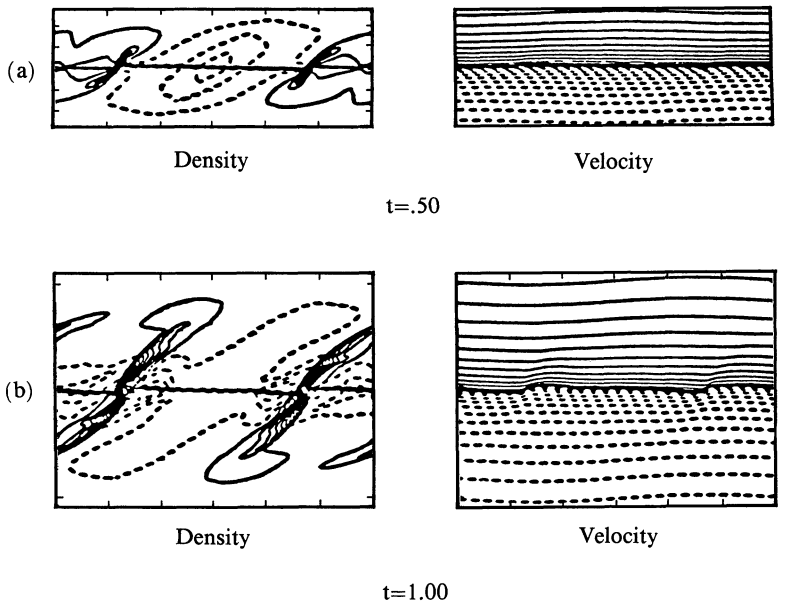

FIGURE 9. The density and velocity profiles at (a) $t = 0.50$ and (b) $t = 1.00$.

of Krasny's calculations, there are explicit examples where a weak solution of the 1-D Vlasov-Poisson equations bursts at a critical time into a measure-valued solution with concentrations in the charge density. In a very precise sense certain weak solutions of the 1-D Vlasov-Poisson equations have analogous but much simpler behavior than 2-D Euler. This is being developed in a forthcoming paper of the author [**64**].

(B) *The nonlinear development of instability for supersonic vortex sheets.* I begin this section by giving some graphs from numerical calculations of Paul Woodward [**65**, **66**, **67**] involving initial data consisting of small amplitude perturbations of the supersonic vortex sheet in (4.1) at Mach number $M = 1.5$. Figures 9 (above) and 10–12 (pages 388–390) give the density contours and velocity contours of the solution that evolves at the successive times $0.50 \leq t \leq 500$. The density contours are on the left in each figure.

It is clear from this sequence of pictures that the small amplitude perturbation grows into a large amplitude instability in the basic vortex sheet from (4.1) by the finite time, $t = 5.00$. Furthermore, one can see the nature of the instability process. By the time $t = 1.50$, kinks have formed in the surface; these kinks are accompanied by a rarefaction wave (depicted by the fan in the density contour on one side of the vortex sheet) and a shock wave (depicted by the abrupt black lines indicating discontinuities in the density contour) and occur in pairs due to symmetry in the initial data. The reader might recall the solutions in (1.13B) at this point. These "kink modes" travel

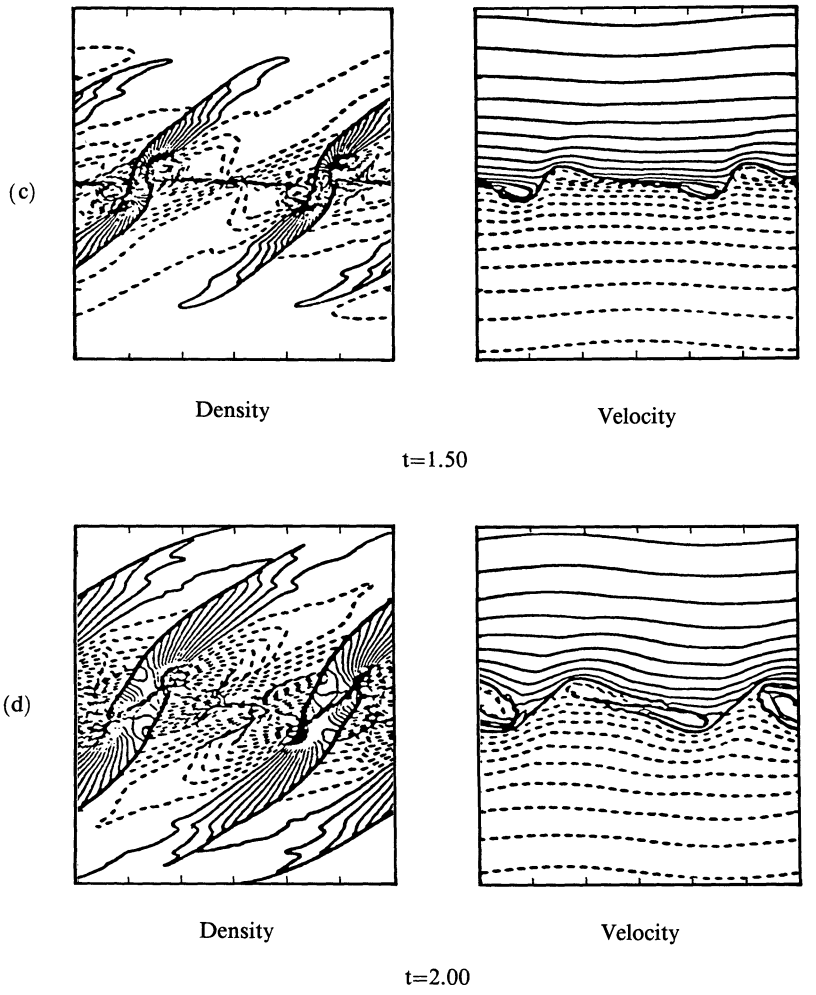

FIGURE 10. The density and velocity profiles at (c) $t = 1.50$ and (d) $t = 2.00$.

along the vortex sheet at different speeds and collide and generate more kink modes with a similar structure by the time $t = 5.00$ as depicted in Figures 10–12. The velocity contours show that an ever increasing amount of vorticity has been generated from the nonlinear interaction of the kink modes. When the calculations are continued beyond time $t = 5.00$, enough vorticity is generated through the interaction of the kink modes that the vortex sheet eventually develops rolls much like the situation described earlier with $M \ll 1$. In numerical computations of Woodward with $M < \sqrt{2}$, the kink modes never appear at small amplitudes and the vortex sheet develops the expected nonlinear Kelvin-Helmholtz instability.

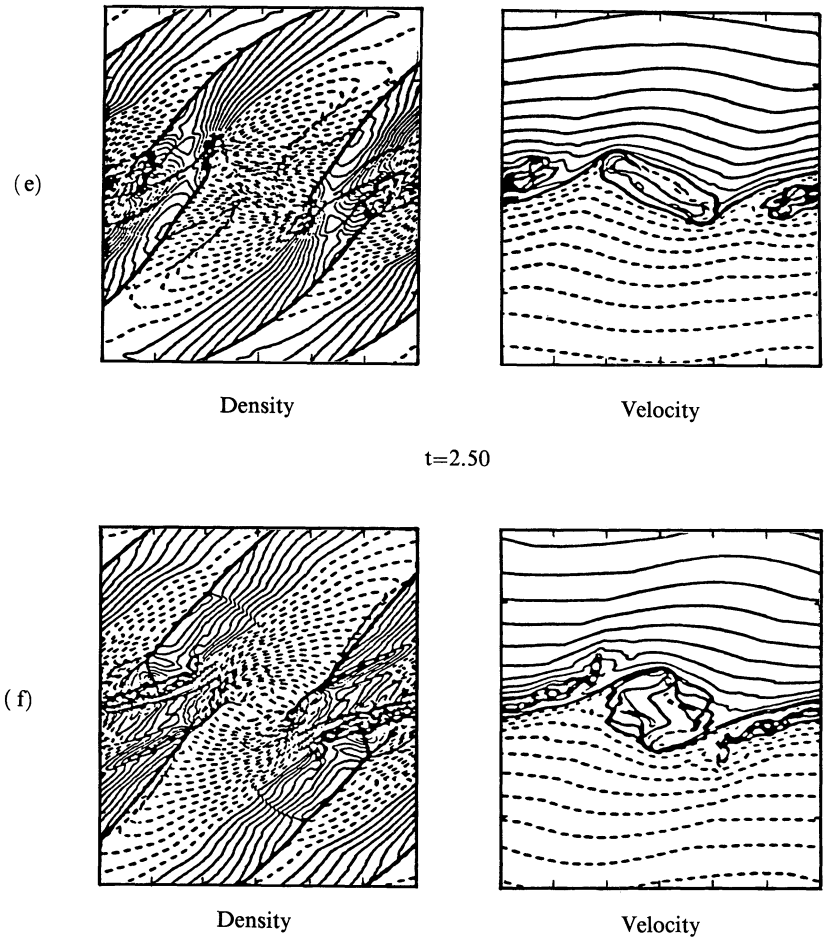

FIGURE 11. The density and velocity profiles at (e) $t = 2.50$ and (f) $t = 3.00$.

The calculations of Woodward suggest the following theoretical questions:

(4.13) Why do "kink" modes form on supersonic vortex sheets? Once such modes form, how do they interact to generate increasing vorticity? What are the quantitative conditions for the formation of kink modes?

Since kink modes are very complicated nonlinear structures simultaneously involving kinks in the vortex sheet bracketed by shock and rarefaction waves, the answers to these questions are not apparent. Furthermore, there is an interesting

PARADOX. The classical engineering and physics linearized stability analysis predicts no growing modes and stability for Mach numbers $M > \sqrt{2}$.

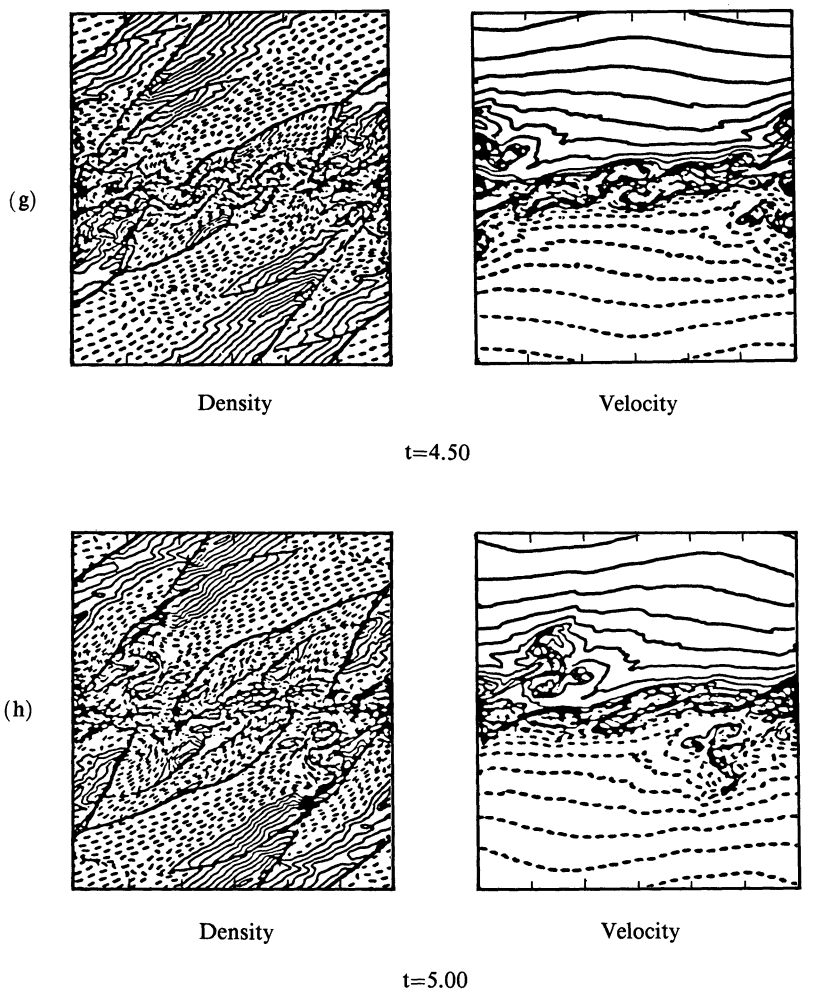

FIGURE 12. The density and velocity profiles at (g) $t = 4.50$ and (h) $t = 5.00$.

The author and his recent Ph.D. student M. Artola have developed a program which answers all of the questions posed in (4.13) and resolves the paradox just mentioned [**68**, **69**, **70**]. This program has three parts:

(1) A quantitative explanation for the appearance of three different families of travelling kink modes at small amplitudes for $M > \sqrt{2}$ together with quantitative prediction of the complete small amplitude shock and rarefaction struction [**68**].

(2) A quantitative theory for the resonant nonlinear interaction of kink modes at the boundary including the increase in vorticity from interaction of the kink modes [**69**].

(3) Exact solutions of the fluid equations given by kink structures at both

large and small amplitudes via bifurcation analysis [**70**].

I do not have the space to develop any of the parts of this program in detail here; however, I make a few comments regarding the methods and results in each part.

In Part (1), the methods of nonlinear geometric optics are generalized to apply to the complex free surface problem defined by the perturbed vortex sheet. Through geometric optics, nonlinear sound waves are generated which strike the vortex sheet and a parameter, the angle of incidence, is varied. For most angles of incidence the response is a transmitted nonlinear sound wave and a reflected nonlinear sound wave with the same magnitude as the incident wave. However, *for* $M > \sqrt{2}$, *there are three angles of incidence where nonlinear resonance occurs and the transmitted and reflected sound waves* are an order of magnitude larger. For these three critical directions, simplified asymptotic equations are obtained for the resonant response in a more sophisticated but similar fashion as described in §2(C). The simplified asymptotic equations consist of an appropriate Hamilton-Jacobi equation for the vortex sheet perturbation coupled with boundary value problems for two nonlinear transport equations as in (2.29) for the reflected and transmitted sound waves. These equations are readily solved exactly and automatically predict the time dependent development of three distinct types of kink modes for $M > \sqrt{2}$. For $1 < M < \sqrt{2}$, there is only a single type of kink mode and for $M < 1$, no such kink modes exist. The details are presented in [**68**].

In Part (2) a theory for resonant interaction of kink modes is developed. Since for $M > \sqrt{2}$ there are three kink modes, it is possible for these kink modes to resonantly interact and generate more vorticity. The arguments in [**69**] are extremely technical since there are double resonances involved—the kink modes are generated by boundary resonances and simultaneously resonantly interact with each other. The result of this technical analysis is an interesting set of simplified asymptotic equations for the resonant interaction of kink modes. These equations for the resonant interaction on the vortex sheet consist of Hamilton-Jacobi equations coupled through resonant integro-differential convolution operators in a fashion already described in (2.31)—one important difference is that the convolution operators in this case are symmetric and allow rapid local amplification. This local amplification is coupled to the growth of vorticity automatically through the asymptotics. Exact solutions of these asymptotic equations display the rapid production of vorticity through these resonant effects as observed in Woodward's calculations.

Finally, I discuss Part (3) of the program [**70**]. Here classical oblique wave theory from [**2**] is utilized to solve a bifurcation problem for exact solutions of the fluid equations consisting of kink modes. Unlike the arguments in Parts (1) and (2), time does not enter explicitly in this steady state analysis. These exact solutions are used at small amplitudes to provide a completely independent confirmation of the time dependent arguments in Part (1). The

exact solutions are also used at large amplitudes to explain the computational results of Woodward for Mach numbers satisfying $1 < M < \sqrt{2}$. In this regime kink modes are not observed at small amplitudes but only at large amplitudes in a very specific way in Woodward's computations and the special nature of the bifurcation diagrams in this regime explains this phenomena.

The graphs from Figures 9–12 are from the early unpublished calculations of Woodward. Recently [**67**] he has confirmed the quantitative predictions of Part (1) in detailed calculations and has generated a color movie with this and other interesting results.

Acknowledgment. The author thanks P. Colella, R. Krasny, M. Shelley, and P. Woodward for the use of unpublished graphs from their numerical simulations.

BIBLIOGRAPHY

1. M. Van Dyke, *An album of fluid motion*, Parabolic Press, Stanford, CA, 1982.
2. R Courant and K. Friedrichs, *Supersonic flow and shock waves*, Springer-Verlag, New York, 1949.
3. A Majda, *Compressible fluid flow and systems of conservation laws in several space variables*, Appl. Math. Sciences, vol. 53, Springer-Verlag, New York, 1984.
4. P. Lax, *Hyperbolic systems of conservation laws*. II, Comm. Pure Appl. Math. **10** (1957), 537–567.
5. ——, *Shock waves and entropy*, Contributions to Nonlinear Functional Analysis (E. A. Zarantonello, ed.), Academic Press, New York, 1971.
6. ——, *Hyperbolic systems of conservation laws and the mathematical theory of shock waves*, Regional Conf. Ser. Appl. Math., No. 13, SIAM, Philadelphia, 1973.
7. J. Glimm, *Solutions in the large for nonlinear hyperbolic systems of equations*, Comm. Pure Appl. Math. **18** (1965), 697–715.
8. J. Smoller, *Shock waves and reaction diffusion equations*, Springer-Verlag, New York, 1983.
9. J. Glimm and P. Lax, *Decay of solutions of systems of nonlinear hyperbolic conservation laws*, Mem. Amer. Math. Soc., No. 101, Amer. Math. Soc., Providence, RI, 1970.
10. T. P. Liu, *Admissible solutions to systems of conservation laws*, Mem. Amer. Math. Soc., No. 240, Amer. Math. Soc., Providence, RI, 1982.
11. C. Dafermos, *Hyperbolic systems of conservation laws*, Systems of Nonlinear Partial Differential Equations (J. Ball, ed.), Reidel, Boston, 1983, pp. 25–70.
12. A. Chorin, *Random choice solutions of hyperbolic systems*, J. Comput. Phys. **22** (1976), 517–533.
13. H. Weyl, *Shock waves in arbitrary fluids*, Comm. Pure Appl. Math. **2** (1949), 103–122.
14. D. Gilbarg, *The existence and limit behavior of the one dimensional shock layer*, Amer. J. Math. **7** (1951), 256–274.
15. R. Pego, *Nonexistence of a shock layer in gas dynamics with a nonconvex equation of state*, Arch. Rational Mech. Anal. **94** (1986), 165–178.
16. A. Majda and R. Pego, *Stable viscosity matrices for systems of conservation laws*, J. Differential Equations **56** (1985), 229–262.
17. T. P. Liu, *Shock waves for compressible Navier-Stokes equations are stable*, Comm. Pure Appl. Math. **39** (1986), 565–594.
18. ——, *Nonlinear stability of shock waves for viscous conservation laws*, Mem. Amer. Math. Soc., no. 328, Amer. Math. Soc., Providence, RI, 1985.
19. J. Goodman, *Nonlinear asymptotic stability of viscous shock profiles for conservation laws*, Arch. Rational Mech. Anal. **95** (1986), 325–344.
20. T. P. Liu and D. Hoff, *The inviscid limit for the Navier-Stokes equations of compressible isentropic flow with shock data*, preprint, 1988.

21. L. Tartar, *Compensated compactness and applications to partial differential equations*, Research Notes in Mathematics, Nonlinear Analysis and Mechanics: Heriot-Watt Symposium, vol. 4 (R. Knops, ed.), Pitman, London, 1979.
22. F. Murat, *Compacite par compensation*, Ann. Scuola Norm. Sup Pisa Cl. Sci. (4) **5** (1978), 69–102.
23. R. DiPerna, *Convergence of approximate solutions to conservation laws*, Arch. Rational Mech. Anal. **82** (1983), 27–70.
24. ——, *Convergence of the viscosity method for isentropic gas dynamics*, Comm. Math. Phys. **91** (1983), 1–30.
25. ——, *Uniqueness of solutions to hyperbolic conservation laws*, Indiana Univ. Math. J. **28** (1979), 137–188.
26. A. Majda, *The stability of multi-dimensional shock fronts*, Mem. Amer. Math. Soc., No. 275, Amer. Math. Soc., Providence, RI, 1983.
27. ——, *The existence of multi-dimensional shock fronts*, Mem. Amer. Math. Soc., No. 281, Amer. Math. Soc., Providence, RI, 1983.
28. G. Metevier, *Interaction de deux chocs pour un systeme de deux lois de conservation en dimension deux d'espace*, Trans. Amer. Math. Soc. **296** (1986), 431–479.
29. S. Alinhac, *Existence d'ondes de rarefaction pour des systemes quasilineares hyperboliques multidimensionnels*, preprint, 1988.
30. E. Harabetian, Ph.D. thesis, U.C.L.A., 1985.
31. A. Majda and E. Thomann, *Multi-dimensional shock fronts for second order wave equations*, Comm. Partial Differential Equations **12** (1987), 777–828.
32. R. Courant and D. Hilbert, *Methods of mathematical physics, Vol.* II, Wiley, New York, 1962.
33. Y. Choi and A. Majda, *Amplification of small amplitude high frequency waves in a reactive mixture*, SIAM Rev. **31** (1989), 401–442.
34. A. Majda, *Lectures on linear and nonlinear hyperbolic waves*, Graduate course, Princeton University, 1986.
35. M. J. Lighthill, *A method for rendering approximate solutions to physical problems uniformly valid*, Philos. Mag. **40** (1949), 1179–1201.
36. G. Whitham, *The flow pattern of a supersonic projectile*, Comm. Pure Appl. Math. **5** (1952), 301–348.
37. Y. Choquet-Bruhat, *Ondes asymptotiques et approchees pour des systemes d'equations aux derivees partielles non lineaires*, J. Math. Pures Appl. **48** (1969), 117–158.
38. J. K. Hunter and J. B. Keller, *Weakly nonlinear high frequency waves*, Comm. Pure Appl. Math. **36** (1983), 547–569.
39. A. Majda, *Nonlinear geometrical optics for hyperbolic systems of conservation laws*, The I.M.A. Volumes in Mathematics and Its Applications, vol. 2, Springer-Verlag, New York, 1986, pp. 116–166.
40. A. Majda and R. Rosales, *Resonantly interacting weakly nonlinear hyperbolic waves*, I: *A single space variable*, Stud. Appl. Math. **71** (1984), 149–179.
41. J. K. Hunter, A. Majda, and R. Rosales, *Resonantly interacting, weakly nonlinear, hyperbolic waves* II: *Several space variables*, Stud. Appl. Math. **75** (1986), 187–226.
42. P. Cehelsky and R. Rosales, *Resonantly interacting weakly nonlinear hyperbolic waves in the presence of shocks: a single space variable in a homogeneous time independent medium*, Stud. Appl. Math. **74** (1986), 117–138.
43. A. Majda, R. Rosales, and M. Schonbek, *A canonical system of integro-differential equations arising in resonant nonlinear acoustics*, Stud. Appl. Math. **79** (1988), 205–262.
44. H. Glaz, P. Colella, I. I. Glass, and R. Deschambault, *A detailed numerical, graphical, and experimental study of oblique shock wave reflections*, Lawrence Berkeley Report, April 1985.
45. C. S. Morawetz, *On the non-existence of continuous transonic flows past profiles*. I, II, III, Comm. Pure Appl. Math. **9** (1956), 45–68; **10** (1957), 107–132; **11** (1958), 129–144.
46. J. Grove, *The interaction of shock waves with fluid interfaces*, preprint, 1988.
47. J. Grove and J. Glimm, private communication.
48. D. Ebin, *The motion of slightly compressible fluids viewed as motion with a strong constraining force*, Ann. of Math. (2) **150** (1977), 102–163.

49. S. Klainerman and A. Majda, *Singular limits of quasilinear hyperbolic systems with large parameters and the incompressible limit of compressible fluids*, Comm. Pure Appl. Math. **34** (1981), 481–524.
50. ____, *Compressible and incompressible fluids*, Comm. Pure Appl. Math. **35** (1982), 629–653.
51. A. Majda, *Vorticity and the mathematical theory of incompressible fluid flow*, Comm. Pure Appl. Math. **39** (1986), S 187–220.
52. J. T. Beale, T. Kato, and A. Majda, *Remarks on the breakdown of smooth solutions for the 3-D Euler equations*, Comm. Math. Phys. **94**, (1984), 61–66.
53. A. J. Chorin, *Spectrum, dimension and polymer analogies in fluid turbulence*, Phys. Rev. Lett. **60** (1988), 1947–1949.
54. V. Yakhot and S. Orszag, *Renormalization group analysis of turbulence* I. *Basic theory*, J. Sci. Comput. **1** (1986), 3–51.
55. C. Sulem, P. Sulem, C. Bardos, and U. Frisch, *Finite time analyticity for the two and three dimensional Kelvin-Helmholtz instability*, Comm. Math. Phys. **80** (1981), 485–516.
56. P. Saffman and G. Baker, Ann. Rev. Fluid Mech. **11** (1979), 95–122.
57. R. Krasny, *Computation of vortex sheet roll-up in the Treffitz plane*, J. Fluid Mech. (1987).
58. M. Shelley and G. Baker, *On the connection between thin vortex layers and vortex sheets*, J. Fluid Mech. (1990), 161–194, Cambridge University Press.
59. R. DiPerna and A. Majda, Comm. Math Phys. **108** (1987), 667–689.
60. ____, *Concentrations in regularizations for 2-D incompressible flow*, Comm. Pure Appl. Math. **60** (1987), 301–345.
61. ____, *Reduced Hausdorff dimension and concentration-cancellation for 2-D incompressible flow*, J. Amer. Math. Soc. **1** (1988), 59–95.
62. A. Majda, *Vortex sheets, potential theory and concentration-cancellation for 2-D incompressible flow*, Princeton lecture notes, 1988.
63. C. Greengard and E. Thomann, *On DiPerna-Majda concentration sets for two-dimensional incompressible flow*, Comm. Pure Appl. Math. **61** (1988).
64. A. Majda, *Concentrations in electron sheets for the 1-D Vlasov-Poisson equations*, in preparation.
65. P. Woodward, in *Numerical methods for the Euler equations of fluid dynamics* (Angrand, Dewieux, Desideri, and Glowinski, eds.), SIAM, Philadelphia, PA, 1985.
66. ____, in *Astrophysical radiation hydrodynamics* (K. H. Winkler and M. Norman, eds.), Reidel, 1986.
67. P. Woodward and K. H. Winkler, *Simulation and visualization of fluid flow in a numerical laboratory*, preprint, October 1988.
68. M. Artola and A. Majda, *Nonlinear development of instabilities in supersonic vortex sheets* I: *the basic kink modes*, Physica D **28** (1988), 253–281.
69. ____, *Nonlinear development of instabilities in supersonic vortex sheets* II: *resonant interaction among kink modes*, SIAM J. Appl. Math. **49** (1989), 1310–1349.
70. ____, *Nonlinear kink modes for supersonic vortex sheets*, Phys. Fluids A **1** (1989), 583–596.
71. R. DiPerna and A. Majda, *The validity of nonlinear geometric optics for weak solutions of conservation laws*, Comm. Math. Phys. **98** (1985), 313–347.

DEPARTMENT OF MATHEMATICS AND PROGRAM IN APPLIED AND COMPUTATIONAL MATHEMATICS, PRINCETON UNIVERSITY, PRINCETON, NEW JERSEY 08544